BER Analysis of IRS-Assisted Wireless Communications in Generalized Gaussian Noise

DOI:
10.1109/TVT.2023.3332812

Document Version
Accepted author manuscript

BER Analysis of IRS-Assisted Wireless Communications in Generalized Gaussian Noise

Ahmad Massud Tota Khel, and Khairi Ashour Hamdi, *Senior Member, IEEE*

***Abstract*—This paper considers intelligent reflecting surface (IRS)-assisted wireless communication systems having an arbitrary number of reflecting elements in additive white generalized Gaussian noise and general fading channels. It presents unified expressions for the precise bit error rate (BER) analysis of different modulation schemes, including M-ary pulse amplitude modulation (MPAM), M-ary quadrature amplitude modulation (MQAM), and M-ary phase shift keying modulation (MPSK). By applying the unified expressions, we analyze the BER performance in different IRS transmission schemes: intelligent transmission, where the phases of the fading channels are known at the IRS; transmission with imperfect phase shifts, where the phases are partially known and/or the IRS is able to apply discrete phase shifts; and blind transmission, where the phases are unknown at the IRS. The preciseness of the expressions is then verified by Monte-Carlo simulations. Although an IRS with blind transmission achieves a higher BER, it can be a promising candidate for low-cost and low-data rate communications through an ambient IRS that does not require implementation complexity and channel estimation overhead.**

***Index Terms*—Arbitrary number of reflecting elements, bit error rate, general fading channels, generalized Gaussian noise, intelligent reflecting surfaces.**

I. Introduction

THE propagation environment in conventional wireless communications itself is random and uncontrollable, which is a major limiting factor and leads to significant performance degradation [1]. In order to manipulate and control the wireless environment, intelligent reflecting surfaces (IRSs) have been introduced which revolutionize the design of future wireless systems. An IRS is composed of a number of nearly passive reflecting elements (REs), which offers the ability to smartly modify the propagation environment and provides indirect transmission paths to wireless systems. Based on the availability of IRS fading channels' phases, the REs apply phase shifts to form beams and direct the incident signals towards a desired destination, and thus the received signal and overall performance are significantly improved [1], [2].

In IRS-assisted systems, when the phases of the fading channels are fully known at the IRS, and the REs apply continuous phase shifts to optimize and align the phases, resulting in signal-to-noise ratio (SNR) maximization, the IRS transmission is referred to as intelligent transmission [3]–[10]. Moreover, when the phases are partially known at the IRS and/or the IRS is able to apply discrete phase shifts, the incident signals are reflected with phase shift errors, which improves the SNR but not maximizes it, and thus it is referred to as transmission with imperfect phase shifts [11]–[14]. On the other hand, when the phases are not known at the IRS, the REs do not apply phase shifts but blindly reflect the incident signals, which is referred to as blind transmission [15]–[18].

In the design and analysis of wireless communications, it has conventionally been assumed that the received signals are impacted solely by additive white Gaussian noise (AWGN), which accounts only for thermal noise. In fact, the background noise in various practical systems can arise from non-Gaussian noise sources as well, that follow distributions with heavier tails than Gaussian distribution [19]–[25]. For instance, man-made interference noise, natural noise, atmospheric noise due to thunderstorms and lighting, noise due the interference signals that appear as short-term random bursts in ultra wide-band wireless systems such as millimeter wave (mmWave) and terahertz (THz) communications, as well as non-Gaussian noise sources in wireless sensor networks, indoor and outdoor wireless systems, wireless-powered communications, and so forth [19]–[25]. Therefore, for an accurate analysis of wireless systems, additive white generalized Gaussian noise (AWGGN), which follows the generalized Gaussian distribution, is used to model different types of noise such as AWGN, gamma noise, and Laplacian noise [19], [23]–[25].

A. Related Works

Since IRSs are envisioned as a promising contender for future wireless systems, the error rate performance of IRS-assisted systems under AWGN, specific fading channels, and a specific transmission scheme has been extensively analyzed [3]–[14], [16]–[18]. In more details, the authors in [3] have analyzed the symbol error rate (SER) of differential phase shift keying modulation for an IRS-assisted system with intelligent transmission under AWGN and Rician fading channels. In [4]–[7], the SER of M-ary phase shift keying (MPSK) modulation for IRS-assisted systems with intelligent transmission over AWGN and Rayleigh fading channels has been studied. In [8] and [9], the SER performance of IRSs-assisted systems with intelligent transmission in the presence of AWGN under Rayleigh and Nakagami-m fading channels has been analyzed, respectively. Moreover, the bit error rate (BER) performance of an IRS-assisted system with binary phase shift keying (BPSK) modulation and intelligent transmission under AWGN and extended η-μ fading channels has been evaluated in [10].

Manuscript received xxxxx xx, 2023; revised xxxxxx xx, 2023; accepted xxxxxxx xx, 2023. Date of publication xxxxxx xx, 2023; date of current version xxxxxxx xx, 2023. The associate editor coordinating the review of this manuscript and approving it for publication was xxxxxxx xxxxxxxx. *(Corresponding author: Ahmad Massud Tota Khel.)*

The authors are with the Department of Electrical and Electronic Engineering, The University of Manchester, Manchester M13 9PL, United Kingdom (e-mail: ahmadmassud.totakhel@postgrad.manchester.ac.uk; k.hamdi@manchester.ac.uk).

In [11] and [12], by considering the IRS transmission with imperfect phase shifts, the approximate SER performance of IRS-assisted systems with different modulation formats over AWGN and Rayleigh fading channels has been studied. In [13], the approximate SER performance of IRS-assisted systems with imperfect phase shifts under AWGN and Rician fading channels has been studied. Moreover, the authors in [14] have analyzed the BER of BPSK modulation for an IRS-assisted system with imperfect phase shifts under AWGN and Nakagami-m fading channels. In [16], by considering MPSK modulation, the SER performance of IRS-assisted wireless communication systems with blind transmission scheme in the presence of AWGN and zero-mean complex Gaussian fading channels has been investigated. In [17], the pairwise error probability of an IRS-assisted system in blind transmission under AWGN and non-zero mean complex Gaussian fading channels has been assessed. In [18], the BER performance of IRS-assisted systems with blind transmission under AWGN and Nakagami-m fading channels has been investigated.

On the other hand, a very limited number of studies has been reported on the BER/SER analysis of IRS-assisted systems under AWGGN [19]–[21]. In further details, the authors in [19] have considered an IRS-assisted system with intelligent transmission under AWGGN and Rayleigh fading channels, and have assessed the approximate SER of the system. In [20], an IRS has been utilized as an access point, where the communication has been assumed to be established through intelligent transmission over Rayleigh fading channels. By considering the AWGN plus Laplacian noise and BPSK modulation, the authors have analyzed the approximate BER performance of the system. Moreover, the authors in [21] have considered BPSK modulation and studied the BER performance of an IRS-assisted system under impulsive noise, intelligent transmission, and Weibull fading channels.

B. Motivations, Contributions, and Organization

The vast majority of the aforementioned literature is based on the assumption of classical AWGN (e.g. [3]–[14], [16]–[18]). Nevertheless, in many applications of wireless communications, relying solely on the assumption of AWGN to describe the noise model is inadequate and neglects other important sources of noise [19]–[25]. Additionally, despite the Gaussian and generalized Gaussian distributions having the same symmetry properties, the heavier-tailed noise types that arise in different wireless environments cannot be modeled by the Gaussian distribution [22], [25]. Therefore, to conduct a precise analysis of IRS-assisted wireless systems, it is necessary to consider a generalized noise model that accurately characterizes various types of noise.

All of the works discussed in Section I-A have analyzed the approximate BER/SER of IRS-assisted systems in specific IRS transmission and fading channels. However, IRSs may operate in different transmission schemes, including intelligent transmission, transmission with imperfect phase shifts, and blind transmission, which are determined based on the availability or lack of the fading channels' phase information. Furthermore, considering the practical applications of wireless systems, IRSs may operate in various wireless environments and scenarios, such as clear line-of-sight (LOS) scenarios, scattering and non-LOS scenarios, indoor and outdoor communications, mmWave and THz communications under different fading conditions, and so forth. Therefore, a generalized framework is needed to accurately analyze the BER of IRS-assisted systems, which can be applied to different transmission schemes and arbitrary types of fading channels.

In addition, several existing works have analyzed the performance of IRS-assisted systems using the central limit theorem-based Gaussian approximation, which relies on the assumption of a large number of REs (e.g. [4]–[8], [14], [16], [17]). Whereas, in practice, due to possible blockages, design requirements and/or hardware failure, a large number of REs might not be always available, which implies the inappropriateness of the Gaussian approximation. To the best of the authors' knowledge, a precise framework for the BER analysis of IRS-assisted systems with M-ary modulation formats and an arbitrary number of REs over general fading channels has not been reported. Moreover, it is noteworthy that the BER behavior of IRS-assisted systems in different IRS transmission schemes has not been compared and investigated. In addition, the impacts of the location of IRS and angle of incidence on the BER performance in different transmission schemes and noise models have not been studied.

Driven by the aforementioned factors, this paper describes its primary contributions and organization as follows.

- In Section II, we consider an IRS-assisted single-antenna wireless communication system with an arbitrary number of REs in general fading channels and AWGGN. The IRS is assumed to operate under various transmission schemes, including intelligent transmission, transmission with imperfect phase shifts, and blind transmission.
- In Section III, we derive unified expressions in terms of the characteristic functions (CHFs) of the end-to-end channel amplitude that facilitate a precise BER analysis of various M-ary modulation schemes, including M-ary pulse amplitude modulation (MPAM), M-ary quadrature amplitude modulation (MQAM), and MPSK modulation over AWGGN. Moreover, as the special cases of AWGGN, further simplified expressions for the precise BER analysis of IRS-assisted systems subject to the well-known AWGN and Laplacian noise are derived.
- In Section IV, taking into account different IRS transmission schemes, accurate CHF expressions for various fading channels such as double Rayleigh, double Nakagami-m, double α-μ, double Rician, double Weibull, and the sum of zero/non-zero mean double complex Gaussian random variables (RVs) are derived.
- In Section V, the performance analysis is extended to IRS-assisted multi-antenna systems. More specifically, it is demonstrated that the unified BER expressions are applicable to a multi-antenna receiver/transmitter that employs equal gain combining/equal gain transmission (EGC/EGT) and maximum ratio combining/maximum ratio transmission (MRC/MRT) diversity schemes.
- In Section VI, the BER performance for an arbitrary number of REs and antennas under different fading channels, transmission schemes, diversity schemes, and

noise models is evaluated via numerical and Monte-Carlo simulations. Finally, the work is concluded in Section VII.

The results demonstrate that under different fading channels and conditions, the impact of Laplacian noise on the BER is more dominant. This is due to the smaller shape parameter of the generalized Gaussian distributed RV in Laplacian noise compared to that of AWGN, which implies that in addition to the thermal noise, other sources of non-Gaussian noise that arise in various wireless environments are also taken into account. The results also demonstrate that, under various noise models and fading channels, an IRS with intelligent transmission achieves the lowest BER. This is attributed to the IRS's perfect knowledge of phases, enabling it to form concentrated beams towards the desired destination, which significantly improves the received signal power and BER. In contrast, the system with blind transmission achieves a higher BER compared to other transmission schemes as the IRS blindly reflects the incident signals without phases information. However, it is cost-efficient and can be a promising candidate for low-data rate applications such as the internet of things (IoT) communications as an ambient IRS can be exploited, eliminating the need for the channel estimation overhead and computational complexity.

It is also shown that under various fading channels and noise models, the impact of phase shift quantization errors, resulting from partial knowledge of phases and/or discrete phase shifters of IRSs, can be mitigated by increasing the number of quantization bits and antennas, albeit at the expense of cost and hardware complexity. Finally, the effects of the location of IRS and angle of incidence in different conditions are assessed. It is observed that when the IRS is positioned in the direct sight of the transmitter, where the angle of incidence becomes zero, the lowest BER is achieved by placing it close to either the transmitter or receiver. Otherwise, the lowest BER can be achieved when it is deployed close to the transmitter.

C. Mathematical Notations

$z \sim \mathcal{CN}(\mu, \sigma^2)$ and $z \sim \mathcal{N}(\mu, \sigma^2)$ represent a circularly symmetric complex Gaussian RV and a normal RV with a mean and variance of μ and σ^2, respectively. The notations $|z|$, $\mathrm{P_r}(z)$, $\mathbb{E}[z]$, and $\mathbb{V}[z]$ represent the absolute value, the probability, the expectation operator, and the variance of z, respectively. Moreover, $f_Z(z)$, $\Phi_z(\omega)$, and $\mathrm{Re}\,\Phi_z(\omega)$ represent the probability density function (PDF), the CHF, and the real part of the CHF of z, respectively. In addition, $\Gamma(.)$ is the gamma function [26, Eq. (8.310)], $\Gamma(.,.)$ is the upper incomplete gamma function [26, Eq. (8.350.2)], $L_{\ell/2}(.)$ is the Laguerre polynomial with order $\ell/2$ [26, Eq. (8.970.1)], $K_n(.)$ is the modified Bessel function of the second kind with order n [26, Eq. (8.432.1)], ${}_1F_1[.;.;.]$ is the Confluent hypergeometric function [26, Eq. (9.210.1)], ${}_2F_1[.,.;.;.]$ is the Gauss Hypergeometric function [26, Eq. (9.111)], erfc(.) is the complementary error function [26, Eq. (8.250.4)], $Q_\eta(x)$ is the generalized Gaussian Q-function [24, Eq. (A.1)], $G_{p,q}^{m,n}\left[.\middle|.\ ,\ .\right]$ is the MeijerG function [26, Eq. (9.301)], and $H_{p,q}^{m,n}\left[.\middle|.\ ,\ .\right]$ is the univariate Fox's H-function [27, Eq. (1.2)], respectively.

II. System Model

We consider a wireless communication system in which a transmitter (T) conveys information to a receiver (R)[1]. We assume that due to severe blockage and obstacles, the direct T-R link does not exist [3]–[9]. Therefore, an IRS with a total area of $W \times L$ between T and R is deployed to facilitate the T-R communication, where the IRS is equipped with an arbitrary number of $N = N_W N_L$ REs. Moreover, the size of each RE is expressed as $\frac{W}{N_W} \times \frac{L}{N_L}$ such that $\frac{W}{N_W}, \frac{L}{N_L} \leq \lambda$, where λ represents the wavelength of the incident signal [28]. Let D, d_T, and d_R represent the T-R horizontal distance, the T-IRS distance, and the IRS-R distance, respectively. In addition, assuming that the T-R, IRS-T, or IRS-R distances are considerably larger than the size of the IRS, e.g. D, d_T, or $d_R \geq \frac{2\max\left(W^2, L^2\right)}{\lambda}$, and thus the plane-wave approximation allows for the assumption of identical large-scale path losses across all REs [28]–[33]. As a result, using [28, Eq. (19)] and [28, Eq. (21)], the large-scale path-loss for the T-IRS and IRS-R paths which takes into account the angle of incidence and size of the IRS can be written as

$$\zeta = \frac{G_T G_R}{16\pi^2} \left(\frac{WL}{d_T d_R}\right)^2 \cos^2\psi, \tag{1}$$

where G_T and G_R are the transmit and receive antennas gain, and ψ is the angle of incidence at the IRS.

Let θ_i, h_i and g_i $\forall i = 1, \ldots, N$ respectively represent the phase shift applied by the i-th RE, and the T-IRS and IRS-R fading channel coefficients which are assumed to follow any arbitrary distribution under different transmission schemes. Therefore, the combined received signal at R is written as

$$y = \sqrt{\zeta} \sum_{i=1}^{N} h_i \mathrm{e}^{j\theta_i} g_i \ s + n, \tag{2}$$

where s is a data symbol selected from M-ary modulation constellations with a bit energy of E_b, and n is the additive white noise which is assumed to follow generalized Gaussian distribution with a mean of zero and variance of $N_0/2$.

The PDF of the generalized Gaussian distributed noise is expressed as [24, Eq. (2)]

$$f_{|n|}(x) = \frac{\eta \vartheta_0}{2\sqrt{N_0}\Gamma\left(\frac{1}{\eta}\right)} \exp\left(-\left(\frac{x\vartheta_0}{\sqrt{N_0}}\right)^\eta\right), \tag{3}$$

where $\vartheta_0 = \sqrt{\frac{2\Gamma\left(\frac{3}{\eta}\right)}{\Gamma\left(\frac{1}{\eta}\right)}}$ is the noise power normalization coefficient, and $\eta \in \mathbb{R}^+$ is the shape parameter of the generalized Gaussian distributed RV.

It is to note that from (3), in addition to mean and variance, AWGGN is also characterized by its shape parameter. Therefore, by varying the value of η in (3), different types of noise can be modeled. For instance, the AWGN and Laplacian noise models are obtained by setting $\eta = 2$ and $\eta = 1$, respectively. Moreover, by increasing the value of η, the adverse effects of noise on the received signal is decreased and vice versa [19], [23]–[25].

[1]In this section, for the sake of simplicity and readability, both T and R are assumed to be equipped with a single antenna, where the analysis is extended to the case of multiple antennas in Section V.

III. BER IN AWGGN AND GENERAL FADING CHANNELS

This section derives CHF-based expressions for the precise BER analysis of IRS-assisted systems in different M-ary modulations over AWGGN and general fading channels, which are applicable to different IRS transmission schemes.

A. M-ary Pulse Amplitude Modulation (MPAM)

We first derive a precise BER expression for 4PAM modulation under pure AWGGN. Next, we establish the relationship between the BER in AWGN and the BER in AWGGN. Finally, we generalize the BER expression for MPAM in the presence of AWGGN and fading channels. Therefore, let's consider the constellation diagram shown in Fig. 1, which illustrates the 2-bit equiprobable symbols of 4PAM with Gray coding labeled as $\{s_0, s_1, s_2, s_3\}$, where it has 4 decision regions. Furthermore, $2\mathcal{A}^{\text{PAM}}$ represents the minimum distance between two adjacent symbols, and the magnitude of the signal is independently selected from the set of $\{\pm\mathcal{A}^{\text{PAM}}, \pm 3\mathcal{A}^{\text{PAM}}\}$, where $\mathcal{A}^{\text{PAM}}$ is written as [34, Eq. (2)]

$$\mathcal{A}^{\text{PAM}} = \sqrt{\frac{3E_b \log_2 M}{M^2 - 1}}. \tag{4}$$

Let b_1 and b_2 represent the first and second bits in each symbol, respectively. From Fig. 1, for $b_1 = 0$, a bit error occurs in s_0/s_1 when the magnitude of noise, $|n|$, exceeds $\mathcal{A}^{\text{PAM}}$ or $3\mathcal{A}^{\text{PAM}}$. Similarly, for $b_1 = 1$, a bit error occurs in s_2/s_3 when the magnitude of noise exceeds $\mathcal{A}^{\text{PAM}}$ or $3\mathcal{A}^{\text{PAM}}$. Therefore, the probability that b_1 is in error can be written as

$$P_{b_1} = \frac{2\text{P}_\text{r}\left(|n| > \mathcal{A}^{\text{PAM}}\right) + 2\text{P}_\text{r}\left(|n| > 3\mathcal{A}^{\text{PAM}}\right)}{4}. \tag{5}$$

Now let's consider the second bit, for $b_2 = 0$, a bit error occurs in s_0 and s_3 when the magnitude of noise is greater than $\mathcal{A}^{\text{PAM}}$ but less than $5\mathcal{A}^{\text{PAM}}$. Moreover, for $b_2 = 1$, a bit error occurs in s_1 and s_2 when the magnitude of noise exceeds $\mathcal{A}^{\text{PAM}}$ or $3\mathcal{A}^{\text{PAM}}$. Therefore, the probability that b_2 is in error can be expressed as

$$\begin{aligned} P_{b_2} &= \frac{1}{4}\Big[2\text{P}_\text{r}\left(\mathcal{A}^{\text{PAM}} < |n| < 5\mathcal{A}^{\text{PAM}}\right) + 2\text{P}_\text{r}\left(|n| > \mathcal{A}^{\text{PAM}}\right) \\ &\quad + 2\text{P}_\text{r}\left(|n| > 3\mathcal{A}^{\text{PAM}}\right)\Big] \\ &= \text{P}_\text{r}\left(|n| > \mathcal{A}^{\text{PAM}}\right) + \frac{1}{2}\text{P}_\text{r}\left(|n| > 3\mathcal{A}^{\text{PAM}}\right) \\ &\quad - \frac{1}{2}\text{P}_\text{r}\left(|n| > 5\mathcal{A}^{\text{PAM}}\right). \end{aligned} \tag{6}$$

To find the probability that a bit error occurs in 4PAM, we need to calculate the average of P_{b_1} and P_{b_2} as

$$\begin{aligned} P_e^{\text{4PAM}} &= \frac{1}{2}\left[P_{b_1} + P_{b_2}\right] \\ &= \frac{3}{4}\mathcal{I}_1 + \frac{1}{2}\mathcal{I}_2 - \frac{1}{4}\mathcal{I}_3, \end{aligned} \tag{7}$$

where $\mathcal{I}_1 \triangleq \text{P}_\text{r}\left(|n| > \mathcal{A}^{\text{PAM}}\right)$, $\mathcal{I}_2 \triangleq \text{P}_\text{r}\left(|n| > 3\mathcal{A}^{\text{PAM}}\right)$ and $\mathcal{I}_3 \triangleq \text{P}_\text{r}\left(|n| > 5\mathcal{A}^{\text{PAM}}\right)$.

Since $|n|$ is an AWGGN with a mean of zero and variance of $N_0/2$, where its PDF is given as (3), it can be written that

$$\mathcal{I}_1 = \frac{\eta\vartheta_0}{2\sqrt{N_0}\Gamma\left(\frac{1}{\eta}\right)} \int_{\mathcal{A}^{\text{PAM}}}^{\infty} \exp\left(-\left(\frac{x\vartheta_0}{\sqrt{N_0}}\right)^{\eta}\right) \text{d}x. \tag{8}$$

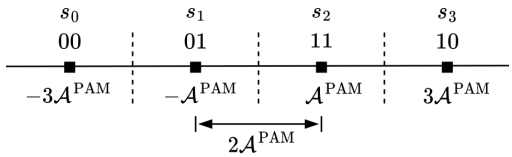

Fig. 1 Constellation diagram for 4PAM with Gray coding.

By interchange of $t = \left(\frac{x\vartheta_0}{\sqrt{N_0}}\right)^{\eta}$, $x = \frac{\sqrt{N_0}t^{\frac{1}{\eta}}}{\vartheta_0}$ and $\text{d}x = \frac{\sqrt{N_0}}{\eta\vartheta_0}t^{\frac{1}{\eta}-1}\,\text{d}t$, (8) is equivalently expressed as

$$\begin{aligned} \mathcal{I}_1 &= \frac{1}{2\Gamma\left(\frac{1}{\eta}\right)} \int_{\left(\frac{\vartheta_0\mathcal{A}^{\text{PAM}}}{\sqrt{N_0}}\right)^{\eta}}^{\infty} \exp\left(-t\right) t^{\frac{1}{\eta}-1} \text{d}t \\ &= \frac{1}{2\Gamma\left(\frac{1}{\eta}\right)} \Gamma\left(\frac{1}{\eta}, \left(\frac{\vartheta_0\mathcal{A}^{\text{PAM}}}{\sqrt{N_0}}\right)^{\eta}\right), \end{aligned} \tag{9}$$

where the integral of (9) is evaluated by [26, Eq. (8.350.2)].

It is worth noting that $\mathcal{I}_2$ and $\mathcal{I}_3$ are derived by following the same steps used for $\mathcal{I}_1$. Therefore, the BER of 4PAM in the presence of pure AWGGN is obtained as

$$\begin{aligned} P_e^{\text{4PAM}} =& \frac{3\Gamma\left(\frac{1}{\eta}, \left(\frac{\vartheta_0\mathcal{A}^{\text{PAM}}}{\sqrt{N_0}}\right)^{\eta}\right)}{8\Gamma\left(\frac{1}{\eta}\right)} + \frac{\Gamma\left(\frac{1}{\eta}, \left(\frac{3\vartheta_0\mathcal{A}^{\text{PAM}}}{\sqrt{N_0}}\right)^{\eta}\right)}{4\Gamma\left(\frac{1}{\eta}\right)} \\ &- \frac{1}{8\Gamma\left(\frac{1}{\eta}\right)} \Gamma\left(\frac{1}{\eta}, \left(\frac{5\vartheta_0\mathcal{A}^{\text{PAM}}}{\sqrt{N_0}}\right)^{\eta}\right). \end{aligned} \tag{10}$$

It is noteworthy that by setting $\eta = 2$ resulting in AWGN, and using the identity $\Gamma\left(1/2, x^2\right)/\Gamma\left(1/2\right) = \text{erfc}\left(x\right)$ [35, Eq. (6.5.17)], the expression given in (10) becomes identical to [34, Eq. (7)] and [36, Eq. (3)]. This establishes a direct relationship between the BER in AWGN and BER in AWGGN. Therefore, by varying the shape parameter of the AWGGN, η, the BER in different types of noise is obtained.

In order to generalize the BER expression for MPAM with Gray coding, the constellation diagram is divided into M decision regions, where the magnitude of the signal is independently selected from the set of $\{\pm\mathcal{A}^{\text{PAM}}, \pm 3\mathcal{A}^{\text{PAM}}, \ldots, \pm(M-1)\mathcal{A}^{\text{PAM}}\}$. Therefore, by following the steps similar to those followed for 4PAM, and using [34, Eq. (9), Eq. (10)] and [36, Eq. (5)], the exact BER for MPAM in pure AWGGN is written as

$$P_e^{\text{MPAM}} = \frac{1}{\log_2 M} \sum_{m=1}^{M-1} \frac{\mathcal{C}_m^{\text{PAM}}\Gamma\left(\frac{1}{\eta}, \left[\frac{(2m-1)\vartheta_0\mathcal{A}^{\text{PAM}}}{\sqrt{N_0}}\right]^{\eta}\right)}{\Gamma\left(\frac{1}{\eta}\right)}, \tag{11}$$

where $\mathcal{C}_m^{\text{PAM}}$ $\forall m = 1, \ldots, (M-1)$ are modulation related coefficients, which are determined based on the constellation size. Moreover, the values of the coefficients for different orders of MPAM in Gray coding are given in [36, TABLE I].

Furthermore, by exploiting [24, Eq. (A.4)] and (4), the exact BER for MPAM in terms of the generalized Gaussian Q-function can be written as

$$P_e^{\text{MPAM}} = \frac{2}{\log_2 M} \sum_{m=1}^{M-1} \mathcal{C}_m^{\text{PAM}}\, Q_\eta\left(\mathcal{B}_m^{\text{PAM}}\sqrt{\frac{E_b}{N_0}}\right), \tag{12}$$

where $\mathcal{B}_m^{\text{PAM}} = (2m-1)\sqrt{\frac{3\log_2 M}{M^2-1}}$.

Since the BER expression given in (12) is based on the assumption of pure AWGGN, E_b/N_0 represents the received SNR per bit in the absence of path-loss and fading channels. Therefore, in order to take into consideration the large-scale path-loss and IRS fading channels, by exploiting the received signal given in (2), the total received SNR is expressed as

$$\begin{aligned}\gamma &= \frac{E_b}{N_0}\zeta\left|\sum_{i=1}^{N} h_i \mathrm{e}^{j\theta_i} g_i\right|^2 \\ &\triangleq \frac{E_b}{N_0}\zeta z^2,\end{aligned} \tag{13}$$

where the total received SNR in different IRS transmission schemes is discussed in Section IV.

Finally, the BER for MPAM in the presence of AWGGN and fading channels is obtained as

$$P_e^{\mathrm{MPAM}} = \frac{2}{\log_2 M}\sum_{m=1}^{M-1} \mathcal{C}_m^{\mathrm{PAM}} \mathbb{E}\left[Q_\eta\left(\mathcal{B}_m^{\mathrm{PAM}}\sqrt{\frac{E_b\zeta}{N_0}}z\right)\right]. \tag{14}$$

B. M-ary Quadrature Amplitude Modulation (MQAM)

Now let's consider the square MQAM modulation scheme with Gray coding, where the equiprobable data symbols in square MQAM consist of two independent components, the in-phase and quadrature components. The magnitude of the signal in both components is independently selected from the set of $\{\pm\mathcal{A}^{\mathrm{QAM}}, \pm 3\mathcal{A}^{\mathrm{QAM}}, \ldots, \pm(\sqrt{M}-1)\mathcal{A}^{\mathrm{QAM}}\}$, where $\mathcal{A}^{\mathrm{QAM}}$ is expressed as [34, Eq. (12)]

$$\mathcal{A}^{\mathrm{QAM}} = \sqrt{\frac{3E_b\log_2 M}{2(M-1)}}. \tag{15}$$

The authors in [34] have derived an exact expression for the BER analysis of square MQAM in the well-known AWGN. Therefore, by exploiting [34, Eq. (14)] and [34, Eq. (16)], the exact BER for square MQAM in pure AWGN is written as

$$\begin{aligned}P_e^{\mathrm{MQAM}} &= \sum_{m=0}^{\sqrt{M}-2} \mathcal{C}_m^{\mathrm{QAM}}\ \mathrm{erfc}\left(\frac{(2m+1)\,\mathcal{A}^{\mathrm{QAM}}}{\sqrt{N_0}}\right) \\ &= \sum_{m=0}^{\sqrt{M}-2} \frac{\mathcal{C}_m^{\mathrm{QAM}}\Gamma\left(\frac{1}{2}, \left(\frac{(2m+1)\mathcal{A}^{\mathrm{QAM}}}{\sqrt{N_0}}\right)^2\right)}{\Gamma\left(\frac{1}{2}\right)},\end{aligned} \tag{16}$$

where $\sum_{m=0}^{\sqrt{M}-2}\mathcal{C}_m^{\mathrm{QAM}} = \frac{1}{2}$ and $\mathcal{C}_m^{\mathrm{QAM}}\ \forall m = 0, 1, \ldots, (\sqrt{M}-2)$ are modulation related coefficients, which are determined based on the constellation size. For example, for 4QAM, 16QAM and 64QAM, the modulation related coefficients are $\mathcal{C}_m^{\mathrm{QAM}} \in \{\frac{1}{2}\}$, $\mathcal{C}_m^{\mathrm{QAM}} \in \{\frac{3}{8}, \frac{2}{8}, \frac{-1}{8}\}$ and $\mathcal{C}_m^{\mathrm{QAM}} \in \{\frac{7}{24}, \frac{6}{24}, \frac{-1}{24}, 0, \frac{1}{24}, 0, \frac{-1}{24}\}$, respectively [37, pp. (631-632)].

It is well known that the error rates in AWGN are computed through the complementary error function or Gaussian Q-function, e.g. [34], [37]–[39]. Based on the relationship between the BER in AWGN and BER in AWGGN shown for (10), and taking into consideration the same symmetry properties of the generalized Gaussian distribution and Gaussian distribution, the error rates in AWGGN are computed by using the generalized Gaussian Q-function [19], [23]–[25]. Therefore, using [24, Eq. (A.4)] and (15), for the case of pure AWGGN, the BER expression given in (16) takes the following form.

$$\begin{aligned}P_e^{\mathrm{MQAM}} &= \sum_{m=0}^{\sqrt{M}-2} \frac{\mathcal{C}_m^{\mathrm{QAM}}}{\Gamma\left(\frac{1}{\eta}\right)}\Gamma\left(\frac{1}{\eta}, \left(\frac{(2m+1)\,\vartheta_0\mathcal{A}^{\mathrm{QAM}}}{\sqrt{N_0}}\right)^\eta\right) \\ &= \sum_{m=0}^{\sqrt{M}-2} 2\mathcal{C}_m^{\mathrm{QAM}}\ Q_\eta\left(\mathcal{B}_m^{\mathrm{QAM}}\sqrt{\frac{E_b}{N_0}}\right),\end{aligned} \tag{17}$$

where $\mathcal{B}_m^{\mathrm{QAM}} = (2m+1)\sqrt{\frac{3\log_2 M}{2(M-1)}}$.

Finally, similar to MPAM, using the total received SNR given in (13), the exact BER for square MQAM in the presence of AWGGN and fading channels is written as

$$P_e^{\mathrm{MQAM}} = \sum_{m=0}^{\sqrt{M}-2} 2\mathcal{C}_m^{\mathrm{QAM}}\ \mathbb{E}\left[Q_\eta\left(\mathcal{B}_m^{\mathrm{QAM}}\sqrt{\frac{E_b\zeta}{N_0}}z\right)\right]. \tag{18}$$

C. M-ary Phase Shift Keying Modulation (MPSK)

First, let's consider the BPSK modulation scheme, by exploiting [39, Eq. (6.6)], the exact BER in the presence of AWGN and fading channels is written as $P_e^{\mathrm{BPSK}} = \frac{1}{2}\mathbb{E}\left[\mathrm{erfc}\left(\sqrt{\frac{E_b\zeta}{N_0}}z\right)\right] = \frac{1}{2\Gamma\left(\frac{1}{2}\right)}\mathbb{E}\left[\Gamma\left(\frac{1}{2}, \left(\sqrt{\frac{E_b\zeta}{N_0}}z\right)^2\right)\right]$. Therefore, similar to MPAM and square MQAM, the BER of BPSK modulation in the presence of AWGGN and fading channels can be written as

$$P_e^{\mathrm{BPSK}} = \mathbb{E}\left[Q_\eta\left(\sqrt{\frac{E_b\zeta}{N_0}}z\right)\right]. \tag{19}$$

It is to note that the exact BER for quadrature phase shift keying (QPSK) modulation is equivalent to that of 4QAM [37]. In addition, the authors in [40] have shown that the BER of coherent MPSK modulation scheme in pure AWGN can be accurately approximated as [40, Eq. (12)]

$$P_e^{\mathrm{MPSK}} = \sum_{m=1}^{\max\left(\frac{M}{4},1\right)} \frac{1}{\max\left(\log_2 M, 2\right)}\ \mathrm{erfc}\left(\mathcal{B}_m^{\mathrm{PSK}}\sqrt{\frac{E_b}{N_0}}\right), \tag{20}$$

where $\mathcal{B}_m^{\mathrm{PSK}} = \sqrt{\log_2 M}\ \sin\left(\frac{(2m-1)\pi}{M}\right)$.

Therefore, similar to MPAM and square MQAM, by exploiting (13) and the identity given in [24, Eq. (A.4)], and by considering the relationship between the BER in AWGGN and BER in AWGN shown for (10), the BER of MPSK modulation in the presence of AWGGN and fading channels in terms of the generalized Gaussian Q-function can be written as

$$P_e^{\mathrm{MPSK}} = \sum_{m=1}^{\max\left(\frac{M}{4},1\right)} \frac{2\mathbb{E}\left[Q_\eta\left(\mathcal{B}_m^{\mathrm{PSK}}\sqrt{\frac{E_b\zeta}{N_0}}z\right)\right]}{\max\left(\log_2 M, 2\right)}. \tag{21}$$

In order to compute the average BER in AWGGN and general fading channels given in (14), (18), (19) and (21), we need to derive the average of the generalized Gaussian Q-function, i.e. $\mathcal{E} \triangleq \mathbb{E}\left[Q_\eta\left(\mathcal{B}\sqrt{\frac{E_b\zeta}{N_0}}z\right)\right]$, where $\mathcal{B} \in \{\mathcal{B}_m^{\mathrm{PAM}}, \mathcal{B}_m^{\mathrm{QAM}}, \mathcal{B}_m^{\mathrm{PSK}}, 1\}$ for MPAM, MQAM, MPSK and BPSK modulations, respectively.

$$\mathcal{E}=\frac{\sqrt{\ell}2^{\frac{1-k}{2}}k^{\frac{2-\eta}{2\eta}}}{\Gamma(1/\eta)\pi^{\frac{k}{2}}}\int_0^{\infty}\frac{\mathrm{Re}\,\Phi_z\left(\omega\right)}{\omega}G_{k+2\ell,2k}^{2k,\ell}\left[\frac{1}{k^k}\left(\frac{2\ell\mathcal{B}}{\omega}\sqrt{\frac{\vartheta_0^2E_b\zeta}{N_0}}\right)^{2\ell}\;\middle|\;\begin{matrix}\frac{1}{2\ell},\ldots,\frac{\ell-\frac{1}{2}}{\ell},\frac{1}{k},\ldots,\frac{1+k-1}{k},0,\ldots,\frac{\ell-1}{\ell}\\0,\ldots,\frac{k-1}{k},\frac{\frac{1}{\eta}}{k},\ldots,\frac{\frac{1}{\eta}+k-1}{k}\end{matrix}\right]\mathrm{d}\omega,\quad(22)$$

Proof: Please refer to Appendix A. ∎

$$\mathcal{E}=\frac{\sqrt{\ell}2^{\frac{3-k}{2}}k^{\frac{2-\eta}{2\eta}}}{\Gamma(1/\eta)\pi^{\frac{k}{2}}}\int_0^{\frac{\pi}{2}}\frac{\mathrm{Re}\,\Phi_z\left(\tan\xi\right)}{\sin 2\xi}G_{k+2\ell,2k}^{2k,\ell}\left[\frac{1}{k^k}\left(\frac{2\ell\mathcal{B}}{\tan\xi}\sqrt{\frac{\vartheta_0^2E_b\zeta}{N_0}}\right)^{2\ell}\;\middle|\;\begin{matrix}\frac{1}{2\ell},\ldots,\frac{\ell-\frac{1}{2}}{\ell},\frac{1}{k},\ldots,\frac{1+k-1}{k},0,\ldots,\frac{\ell-1}{\ell}\\0,\ldots,\frac{k-1}{k},\frac{\frac{1}{\eta}}{k},\ldots,\frac{\frac{1}{\eta}+k-1}{k}\end{matrix}\right]\mathrm{d}\xi.\quad(23)$$

Lemma 1. By exploiting the convolution theorem for the Fourier cosine transform, the average of the generalized Gaussian Q-function is obtained as (22) given at the top of this page. The parameters of (22) are $\eta=\frac{2\ell}{k}$, $\ell\in\mathbb{Z}^+$, $k\in\mathbb{Z}^+$, and $\gcd(k,\ell)=1$, where gcd stands for the greatest common divisor. Moreover, $\mathrm{Re}\,\Phi_z\left(\omega\right)=\frac{\Phi_z(\omega)+\Phi_z(-\omega)}{2}$ is the real part of the CHF for the end-to-end channel amplitude, i.e. $z=\left|\sum_{i=1}^{N}h_i\mathrm{e}^{j\theta_i}g_i\right|$, where the CHF expressions for different transmission schemes and channels are derived in Section IV.

Furthermore, for the sake of an efficient numerical analysis and integration, by interchange of $\omega=\tan\xi$, and after some algebraic manipulations, an alternative expression for (22) is obtained as (23) given at the top of this page. Finally, by substituting (22)/(23) into (14), (18), (19) and (21), the precise average BER of IRS-assisted systems with different modulation schemes and an arbitrary number of REs in the presence of AWGGN and general fading channels is obtained. In addition, as the special cases of AWGGN, we present the average of the generalized Gaussian Q-function, $\mathcal{E}$, in the well-known AWGN and Laplacian noise as follows.

Corollary 1. When $\eta=2$, n in (2) becomes a Gaussian distributed noise or AWGN. Therefore, using $\eta=\frac{2\ell}{k}$, we can write that $\ell=k=1$, and by substituting them into (22) and after some algebraic manipulations, $\mathcal{E}$ is obtained as

$$\mathcal{E}=\int_0^{\infty}\frac{\mathrm{Re}\,\Phi_z\left(\omega\right)}{\pi\omega}\,G_{3,2}^{2,1}\left[\frac{4\mathcal{B}^2\zeta}{\omega^2}\frac{E_b}{N_0}\;\middle|\;\begin{matrix}\frac{1}{2},1,0\\0,\frac{1}{2}\end{matrix}\right]\mathrm{d}\omega.\quad(24)$$

By applying [41, Eq. (07.34.03.0002.01)], (25) is further simplified as

$$\mathcal{E}=\int_0^{\infty}\frac{\mathrm{Re}\,\Phi_z\left(\omega\right)}{\pi\omega}G_{2,1}^{1,1}\left[\frac{4\mathcal{B}^2\zeta}{\omega^2}\frac{E_b}{N_0}\;\middle|\;\begin{matrix}\frac{1}{2},1\\\frac{1}{2}\end{matrix}\right]\mathrm{d}\omega.\quad(25)$$

Moreover, by applying [41, Eq. (07.34.03.0309.01)], and after some algebraic manipulations, (25) can be explicitly expressed as

$$\mathcal{E}=\frac{1}{\sqrt{\pi^3\mathcal{H}}}\int_0^{\infty}\mathrm{Re}\,\Phi_z\left(\omega\right)\;{}_1F_1\left[1;\frac{3}{2};-\frac{\omega^2}{4\mathcal{H}}\right]\mathrm{d}\omega,\quad(26)$$

where $\mathcal{H}\triangleq\mathcal{B}^2\zeta\frac{E_b}{N_0}$.

By interchange of $\omega=\tan\xi$ in (26), a more suitable expression for the numerical integration is obtained as

$$\mathcal{E}=\int_0^{\frac{\pi}{2}}\frac{\mathrm{Re}\,\Phi_z\left(\tan\xi\right)}{\sqrt{\pi^3\mathcal{H}}\cos^2\xi}{}_1F_1\left[1;\frac{3}{2};\frac{-\tan^2\xi}{4\mathcal{H}}\right]\mathrm{d}\xi.\quad(27)$$

It is noteworthy that (26) and (27) are easily evaluated by numerical integration. Moreover, by exploiting [35, Eq. (25.4.45)], (26) can be written in terms of the weight factors and samples points of the Laguerre orthogonal polynomial as

$$\mathcal{E}=\sum_{\jmath=1}^{\mathcal{L}}\frac{\alpha_\jmath\,\mathrm{Re}\,\Phi_z\left(\beta_\jmath\right)}{\sqrt{\pi^3\mathcal{H}}e^{-\beta_\jmath}}\;{}_1F_1\left[1;\frac{3}{2};-\frac{\beta_\jmath^2}{4\mathcal{H}}\right]+\mathcal{R}_{\mathcal{L}},\quad(28)$$

where $\alpha_\jmath$ and $\beta_\jmath$ are respectively the weights factors and sample points of the Laguerre orthogonal polynomial tabulated in [35, Table (25.9)]. Moreover, $\mathcal{R}_{\mathcal{L}}$ is a remainder defined in [35, Eq. (25.4.45)], where for a large $\mathcal{L}$, it approaches zero, and thus it can be neglected.

Corollary 2. When $\eta=1$, n in (2) becomes a Laplacian distributed noise, and thus by exploiting $\eta=\frac{2\ell}{k}$, we can write that $\ell=1$ and $k=2$. By substituting them into (22), and after some algebraic manipulations, the average of the generalized Gaussian Q-function, $\mathcal{E}$, is obtained as

$$\mathcal{E}=\frac{1}{\pi}\int_0^{\infty}\frac{\mathrm{Re}\,\Phi_z\left(\omega\right)}{\omega}\;G_{4,4}^{4,1}\left[\frac{4\mathcal{B}^2\zeta}{\omega^2}\frac{E_b}{N_0}\;\middle|\;\begin{matrix}\frac{1}{2},\frac{1}{2},1,0\\0,\frac{1}{2},\frac{1}{2},1\end{matrix}\right]\mathrm{d}\omega.\quad(29)$$

It is noteworthy that (29) is evaluated through numerical integration. Alternatively, a further simplified expression for (29) is presented as

$$\mathcal{E}=\frac{2\mathcal{B}}{\pi}\sqrt{\frac{\zeta E_b}{N_0}}\int_0^{\infty}\frac{\mathrm{Re}\,\Phi_z\left(\omega\right)}{\omega^2+4\mathcal{B}^2\zeta\frac{E_b}{N_0}}\mathrm{d}\omega.\quad(30)$$

Proof: Please refer to Appendix B. ∎

The integral of (30) is easily evaluated through numerical integration. Furthermore, using [35, Eq. (25.4.45)], it can be expressed in closed-form as

$$\mathcal{E}=\frac{2\mathcal{B}}{\pi}\sqrt{\frac{\zeta E_b}{N_0}}\sum_{\jmath=1}^{\mathcal{L}}\frac{\alpha_\jmath\,\mathrm{Re}\,\Phi_z\left(\beta_\jmath\right)}{e^{-\beta_\jmath}\left(\beta_\jmath^2+4\mathcal{B}^2\zeta\frac{E_b}{N_0}\right)}+\mathcal{R}_{\mathcal{L}},\quad(31)$$

where $\mathcal{R}_{\mathcal{L}}$ is a remainder, $\beta_\jmath$ are sample points, and $\alpha_\jmath$ are the weights factors tabulated in [35, Table (25.9)].

Finally, by substituting (26)/(27) and (30)/(31) into (14), (18), (19) and (21), the average BER of IRS-assisted wireless communication systems with different modulation schemes in the presence of AWGN and Laplacian noise over generalized fading channels are obtained, respectively.

IV. Characteristic Functions for IRS Fading Channels In Different Transmission Schemes

In this section, we present CHF expressions for the end-to-end channel amplitude, $\Phi_z(\omega)$, in different IRS transmission schemes and fading channels to facilitate a precise BER analysis of IRS-assisted wireless communication systems.

A. Intelligent Transmission Scheme

In intelligent transmission, the phases of h_i and g_i are assumed to be fully known at the IRS, and the IRS REs adjust and apply continuous phase shifts to reflect the incident signals with concentrated beams towards R. Let's express the IRS fading channel coefficients in terms of their corresponding amplitudes and phases as $h_i = |h_i| \exp(j \arg(h_i))$ and $g_i = |g_i| \exp(j \arg(g_i))$, where $\{|h_i|, |g_i|\}$ and $\{\arg(h_i), \arg(g_i)\}$ represent the IRS channel amplitudes and phases, respectively. Therefore, in order to fully compensate for the phases and maximize the received SNR, the adjustable continuous phase shifts are set as $\theta_i = -(\arg(h_i) + \arg(g_i)) \; \forall i = 1, \ldots, N$ [4]–[7]. As a result, the total received SNR given in (13) takes the following form.

$$\gamma = \frac{E_b}{N_0} \zeta \left| \sum_{i=1}^{N} |h_i||g_i| \right|^2. \tag{32}$$

From (13) and (32), we can write that $z = \left| \sum_{i=1}^{N} |h_i||g_i| \right| \triangleq \left| \sum_{i=1}^{N} z_i \right|$, where $|h_i|$ and $|g_i|$ are assumed to follow any arbitrary distribution. Moreover, by assuming that z is the sum of mutually independent RVs, it can be written that

$$\Phi_z(\omega) = \prod_{i=1}^{N} \Phi_{z_i}(\omega), \tag{33}$$

where $\Phi_{z_i}(\omega)$ is the CHF of the channel amplitude for a single RE.

If we assume that $z_i \; \forall i = 1, \ldots, N$ are mutually independent and identically distributed, (33) takes the following form.

$$\Phi_z(\omega) = [\Phi_{z_i}(\omega)]^N. \tag{34}$$

In order to derive $\Phi_{z_i}(\omega)$ for different types of fading channels, we provide the following lemmas.

Lemma 2. We assume that $z_i \triangleq |h_i||g_i|$ is the product of two independent non-identically distributed (i.n.id) Rayleigh RVs, and thus its exact CHF is expressed as

$$\Phi_{z_i}(\omega) = {}_2F_1\left[1, 1; \frac{1}{2}; -\frac{\sigma_{h_i}^2 \sigma_{g_i}^2 \omega^2}{4}\right] + j \frac{2\pi\omega}{\sigma_{h_i}^2 \sigma_{g_i}^2} \left(\omega^2 + \frac{4}{\sigma_{h_i}^2 \sigma_{g_i}^2}\right)^{-\frac{3}{2}}, \tag{35}$$

where $\sigma_{h_i}^2$ and $\sigma_{g_i}^2$ are the variances of the complex Gaussian RVs, h_i and g_i, respectively.

Proof: Please refer to Appendix C. ∎

Lemma 3. We assume that $|h_i|$ and $|g_i|$ are two i.n.id $\alpha - \mu$ RVs, and thus $z_i \triangleq |h_i||g_i|$ is a double $\alpha - \mu$ RV, where its exact CHF is expressed as

$$\begin{aligned}\Phi_{z_i}(\omega) &= \mathcal{K} H_{2,2}^{2,1}\left[\frac{2\mu_{h_i}^{\frac{1}{\alpha_{h_i}}} \mu_{g_i}^{\frac{1}{\alpha_{g_i}}}}{\Omega_{h_i}^{\frac{1}{\alpha_{h_i}}} \Omega_{g_i}^{\frac{1}{\alpha_{g_i}}} \omega} \middle| \begin{matrix} \left(1, \frac{1}{2}\right), \left(\frac{1}{2}, \frac{1}{2}\right) \\ \left(\mu_{h_i}, \frac{1}{\alpha_{h_i}}\right), \left(\mu_{g_i}, \frac{1}{\alpha_{g_i}}\right) \end{matrix}\right] \\ &\quad + j\mathcal{K} H_{2,2}^{2,1}\left[\frac{2\mu_{h_i}^{\frac{1}{\alpha_{h_i}}} \mu_{g_i}^{\frac{1}{\alpha_{g_i}}}}{\Omega_{h_i}^{\frac{1}{\alpha_{h_i}}} \Omega_{g_i}^{\frac{1}{\alpha_{g_i}}} \omega} \middle| \begin{matrix} \left(\frac{1}{2}, \frac{1}{2}\right), \left(1, \frac{1}{2}\right) \\ \left(\mu_{h_i}, \frac{1}{\alpha_{h_i}}\right), \left(\mu_{g_i}, \frac{1}{\alpha_{g_i}}\right) \end{matrix}\right],\end{aligned} \tag{36}$$

where $\mathcal{K} = \frac{\sqrt{\pi}}{2\Gamma(\mu_{h_i})\Gamma(\mu_{g_i})}$, α_{h_i} and α_{g_i} are arbitrary fading parameters, μ_{h_i} and μ_{g_i} are the shape parameters, and Ω_{h_i} and Ω_{g_i} are the scaling parameters of $|h_i|$ and $|g_i|$, respectively.

Proof: Please refer to Appendix D. ∎

It is noteworthy that the $\alpha - \mu$ distribution is a generalized fading distribution, where by varying its parameters, different types of fading distributions such as double Nakagami-m, double Gamma and double Weibull distributions can be modeled. More specifically, by setting $\alpha_{h_i} = \alpha_{g_i} = 2$, $\mu_{h_i} = m_{h_i}$ and $\mu_{g_i} = m_{g_i}$, it reduces to double Nakagami-m distribution. Moreover, by setting $\alpha_{h_i} = \alpha_{g_i} = 1$ and the fading parameters as μ_{h_i} and μ_{g_i}, it reduces to double Gamma distribution. In addition, by setting $\mu_{h_i} = \mu_{g_i} = 1$ and the fading parameters as $\alpha_{h_i}/2$ and $\alpha_{g_i}/2$, it reduces to double Weibull distribution [42]–[44].

Corollary 3. By setting $\alpha_{h_i} = \alpha_{g_i} = 2$, $\mu_{h_i} = m_{h_i}$ and $\mu_{g_i} = m_{g_i}$ in (36), and by applying the identities given in [27, Eq. (1.58)] and [27, Eq. (1.59)], the CHF of a double Nakagami-m RV is obtained as

$$\begin{aligned}\Phi_{z_i}(\omega) =& \mathcal{G} H_{2,2}^{2,1}\left[\frac{\chi\omega^2}{4} \middle| \begin{matrix} (1 - m_{h_i}, 1), (1 - m_{g_i}, 1) \\ (0, 1), \left(\frac{1}{2}, 1\right) \end{matrix}\right] \\ &+ j\mathcal{G} H_{2,2}^{2,1}\left[\frac{\chi\omega^2}{4} \middle| \begin{matrix} (1 - m_{h_i}, 1), (1 - m_{g_i}, 1) \\ \left(\frac{1}{2}, 1\right), (0, 1) \end{matrix}\right],\end{aligned} \tag{37}$$

where $\mathcal{G} = \frac{\sqrt{\pi}}{\Gamma(m_{h_i})\Gamma(m_{g_i})}$, $\chi = \frac{\Omega_{h_i}\Omega_{g_i}}{m_{h_i} m_{g_i}}$, $\Omega_{h_i} = \mathbb{E}\left[|h_i|^2\right]$ and $\Omega_{g_i} = \mathbb{E}\left[|g_i|^2\right]$.

In addition, by applying [27, Eq. (1.60)] and [27, Eq. (1.132)], and after some algebraic manipulations, a further simplified expression for (37) is obtained as

$$\begin{aligned}\Phi_{z_i}(\omega) =& {}_2F_1\left[m_{h_i}, m_{g_i}; \frac{1}{2}; -\frac{\chi\omega^2}{4}\right] + j\mathcal{I}\sqrt{\chi\omega^2} \\ &\times {}_2F_1\left[\frac{2m_{h_i}+1}{2}, \frac{2m_{g_i}+1}{2}; \frac{3}{2}; -\frac{\chi\omega^2}{4}\right],\end{aligned} \tag{38}$$

where $\mathcal{I} = \frac{\Gamma\left(\frac{2m_{h_i}+1}{2}\right)\Gamma\left(\frac{2m_{g_i}+1}{2}\right)}{\Gamma(m_{h_i})\Gamma(m_{g_i})}$.

$$\mathbb{E}\left[z^2\right] = N\left(\mathbb{E}\left[|h_i|^2\right]\mathbb{E}\left[|g_i|^2\right] + (N-1)\,\mathbb{E}^2\left[|h_i|\right]\mathbb{E}^2\left[|g_i|\right]\mathcal{F}_1^2\right), \tag{39}$$

$$\begin{aligned}\mathbb{E}\left[z^4\right] =& N\Big\{\mathbb{E}\left[|h_i|^4\right]\mathbb{E}\left[|g_i|^4\right] + (N-1)\,\mathbb{E}^2\left[|h_i|^2\right]\mathbb{E}^2\left[|g_i|^2\right] + (N-1)\Big[2\,(N-2)\,\mathbb{E}\left[|h_i|^2\right]\mathbb{E}\left[|g_i|^2\right]\mathbb{E}^2\left[|h_i|\right]\mathbb{E}^2\left[|g_i|\right]\mathcal{F}_1^2 \\ &\times(1+\mathcal{F}_2) + \mathbb{E}^2\left[|h_i|^2\right]\mathbb{E}^2\left[|g_i|^2\right]\left(1+\mathcal{F}_2^2\right) + (N-2)\,(N-3)\,\mathbb{E}^4\left[|h_i|\right]\mathbb{E}^4\left[|g_i|\right]\mathcal{F}_1^4\Big] + 4\,(N-1)\,\mathbb{E}\left[|h_i|^3\right]\mathbb{E}\left[|g_i|^3\right] \\ &\times\,\mathbb{E}\left[|h_i|\right]\mathbb{E}\left[|g_i|\right]\mathcal{F}_1^2 + 2\,(N-1)\,(N-2)\,\mathbb{E}\left[|h_i|^2\right]\mathbb{E}\left[|g_i|^2\right]\mathbb{E}^2\left[|h_i|\right]\mathbb{E}^2\left[|g_i|\right]\mathcal{F}_1^2\Big\},\end{aligned} \tag{40}$$

where $\mathcal{F}_1 = \frac{2^q}{\pi}\sin\left(\frac{\pi}{2^q}\right)$ and $\mathcal{F}_2 = \frac{2^q}{2\pi}\sin\left(\frac{2\pi}{2^q}\right)$ [45].

B. Transmission With Imperfect Phase Shifts

We assume that the phases of the IRS fading channels are partially known at the IRS and/or the IRS is able to apply a quantized or discrete set of phase shifts. Taking into consideration the practical IRSs with discrete phase shifters, it is assumed that the interval of the phase shift at each RE is equally spaced (i.e. uniformly quantized) into 2^q levels, where q represents the number of quantization bits [12], [13], [45]–[48]. Therefore, the phase shift applied by the i-th RE, θ_i, takes a finite number of discrete values from an equally spaced set of $\mathcal{S} \triangleq \left\{0, \frac{2\pi}{2^q}, \ldots, \frac{2\pi(2^q-1)}{2^q}\right\}$, where this transmission scheme is referred to as transmission with imperfect phase shifts. In this case, the IRS REs cannot precisely estimate the phases, and reflect the incident signals with imperfect phase shifts, i.e. $\theta_i \neq -\left(\arg(h_i) + \arg(g_i)\right)$. Therefore, the received SNR is improved but cannot be maximized, and thus the system suffers from phase shift quantization errors, which are denoted by $\phi_i = \theta_i - \arg(h_i) - \arg(g_i)$ [11]–[13], [45]–[48].

It should be noted that the authors in [13] have mathematically demonstrated that the applied phase shifts and the phase errors follow the same distribution, where it has been confirmed through numerical and simulation results, specifically for the case of uniformly quantized phase shifts. Therefore, as the interval of phase shifts are uniformly quantized into 2^q levels, it follows that the phase shift quantization errors are uniformly distributed in the interval of $\left[-\frac{\pi}{2^q}, \frac{\pi}{2^q}\right]$ [12], [13], [45]–[48]. As a result, the received SNR given in (13), takes the following form.

$$\gamma = \frac{E_b}{N_0}\zeta\left|\sum_{i=1}^{N}|h_i||g_i|e^{j\phi_i}\right|^2. \tag{41}$$

In the case of imperfect phase shifts, from (13) and (41), the end-to-end channel amplitude is expressed as $z = \left|\sum_{i=1}^{N}|h_i||g_i|e^{j\phi_i}\right|$. Since z is a non-negative RV, according to [49, Sec. (2.2.2)], it can be tightly approximated by the first branch of the Laguerre expansion which is equivalent to gamma distribution. The accuracy of this approximation has been verified for different numbers of REs under various fading channels in [12], [33], [45], [50] and [51]. More specifically, its accuracy has been confirmed for IRS-assisted systems under Rayleigh fading channels in [12], Rician fading channels in [33], [45], Nakagami-m fading channels in [50], and Weibull fading channels in [51]. Therefore, by exploiting [38, Table 2.3-3], the CHF of z is expressed as

$$\Phi_z(\omega) = \left(\frac{1}{1-j\omega\alpha_z}\right)^{\beta_z}, \tag{42}$$

where by exploiting [12], the parameters α_z and β_z are respectively expressed as

$$\alpha_z = \sqrt{\frac{\mathbb{E}\left[z^2\right]}{\beta_z\left(\beta_z+1\right)}}, \tag{43}$$

$$\beta_z = \frac{5\left(\mathbb{E}\left[z^2\right]\right)^2 - \mathbb{E}\left[z^4\right] + \delta}{2\mathbb{E}\left[z^4\right] - 2\left(\mathbb{E}\left[z^2\right]\right)^2}, \tag{44}$$

where $\delta \triangleq \sqrt{\left(\mathbb{E}\left[z^4\right]\right)^2 + 14\left(\mathbb{E}\left[z^2\right]\right)^2\mathbb{E}\left[z^4\right] + \left(\mathbb{E}\left[z^2\right]\right)^4}$.

In order to calculate α_z and β_z, we need to derive the second the fourth moments of z in different fading channels. Therefore, by exploiting [12, Appendix A] and [52, Appendix C], we can express $\mathbb{E}\left[z^2\right]$ and $\mathbb{E}\left[z^4\right]$ respectively as (39) and (40), which are provided at the top of this page. Furthermore, to obtain (39) and (40), the moments of $|h_i|$ and $|g_i|$ in different fading channels are required. Therefore, by exploiting [38, Eq. (2.3-45)], [38, Eq. (2.3-59)], [38, Eq. (2.3-70)] and [53, Eq. (4)], the n-th moment of $|h_i|$ and $|g_i|$ in Rayleigh, Rician, Nakagami-m, and Weibull fading channels are expressed as (45), (46), (47), and (48), respectively.

$$\mathbb{E}\left[|x|^n\right] = \sigma_x^n\,\Gamma\left(1+\frac{n}{2}\right),\ x \in \{h_i, g_i\}. \tag{45}$$

$$\mathbb{E}\left[|x|^n\right] = \sigma_x^n\,\Gamma\left(1+\frac{n}{2}\right)L_{\frac{n}{2}}\left(-\frac{\mu_x^2}{\sigma_x^2}\right),\ x \in \{h_i, g_i\}. \tag{46}$$

$$\mathbb{E}\left[|x|^n\right] = \left(\frac{\Omega_x}{m_x}\right)^{\frac{n}{2}}\frac{\Gamma\left(m_x+\frac{n}{2}\right)}{\Gamma\left(m_x\right)},\ x \in \{h_i, g_i\}. \tag{47}$$

$$\mathbb{E}\left[|x|^n\right] = \Omega_x^n\,\Gamma\left(1+\frac{n}{\alpha_x}\right),\ x \in \{h_i, g_i\}. \tag{48}$$

C. Blind Transmission Scheme

Assuming the phases of h_i and g_i are not known at the IRS, and thus the IRS REs do not apply phase shifts but blindly reflect the incident signals, i.e. $\theta_i = 0\ \forall i = 1, \ldots, N$, which is referred to as blind transmission [15]–[18]. In this transmission scheme, one may assume that T exploits an ambient IRS to convey the intended information to R. This can be particularly a promising candidate for cost-constrained

and low-power communications, such as IoT and wireless-powered communications, as it eliminates the need for the channel estimation overhead and reduces the computational complexity. As a result, the received SNR in the blind transmission scheme takes the following form.

$$\gamma = \frac{E_b}{N_0}\zeta \left| \sum_{i=1}^{N} h_i g_i \right|^2 . \tag{49}$$

where by comparing (13) and (49), it can be written that $z \triangleq \left|\sum_{i=1}^{N} h_i g_i\right|$.

We initially assume that the T-IRS and IRS-R fading channel coefficients are zero mean complex Gaussian RVs, i.e. $h_i \sim \mathcal{CN}(0, \sigma_{h_i}^2)$ and $g_i \sim \mathcal{CN}(0, \sigma_{g_i}^2)$. Therefore, considering an arbitrary number of REs, the following lemma presents the CHF of z.

Lemma 4. The exact CHF for the end-to-end channel amplitude, z, in zero mean double complex Gaussian RVs is expressed as

$$\Phi_z(\omega) = {}_2F_1\left[N, 1; \frac{1}{2}; \frac{-\omega^2\sigma_{h_i}^2\sigma_{g_i}^2}{4}\right] + j\frac{\sqrt{\pi}\sigma_{h_i}\sigma_{g_i}\omega}{2\Gamma(N)} \times \Gamma\left(\frac{2N+1}{2}\right) {}_2F_1\left[\frac{2N+1}{2}, \frac{3}{2}; \frac{3}{2}; \frac{-\omega^2\sigma_{h_i}^2\sigma_{g_i}^2}{4}\right]. \tag{50}$$

Proof: Please refer to Appendix E. ∎

Now let's assume that the T-IRS and IRS-R fading channel coefficients are non-zero mean complex Gaussian RVs, i.e. $h_i \sim \mathcal{CN}(\mu_{h_i}, \sigma_{h_i}^2)$ and $g_i \sim \mathcal{CN}(\mu_{g_i}, \sigma_{g_i}^2)$. Moreover, h_i and g_i can be expressed in terms of their corresponding real and imaginary parts as $h_i = h_i^R + jh_i^I$ and $g_i = g_i^R + jg_i^I$, where $h_i^R \sim \mathcal{N}\left(\mu_{h_i}^R, \sigma_{h_i}^2/2\right)$, $h_i^I \sim \mathcal{N}\left(\mu_{h_i}^I, \sigma_{h_i}^2/2\right)$, $g_i^R \sim \mathcal{N}\left(\mu_{g_i}^R, \sigma_{g_i}^2/2\right)$ and $g_i^I \sim \mathcal{N}\left(\mu_{g_i}^I, \sigma_{g_i}^2/2\right)$. Therefore, the following lemma tightly approximates the PDF and CHF of the end-to-end channel amplitude, $z = \left|\sum_{i=1}^{N} h_i g_i\right|$, considering any arbitrary number of REs.

Lemma 5. The PDF and CHF of the end-to-end channel amplitude, z, in non-zero mean complex Gaussian RVs can be respectively expressed as

$$f_Z(z) = \frac{2\Psi z}{\Gamma(\varphi)} G_{0,1}^{1,0}\left[\Psi z^2 \middle| \begin{matrix} - \\ \varphi - 1 \end{matrix}\right], \tag{51}$$

and

$$\Phi_z(\omega) = \frac{\sqrt{\pi}}{\Gamma(\varphi)}\left(G_{2,1}^{1,1}\left[\frac{4\Psi}{\omega^2}\middle| \begin{matrix} 1, \frac{1}{2} \\ \varphi \end{matrix}\right] + jG_{2,1}^{1,1}\left[\frac{4\Psi}{\omega^2}\middle| \begin{matrix} \frac{1}{2}, 1 \\ \varphi \end{matrix}\right]\right), \tag{52}$$

with

$$\Psi = \frac{\mathbb{E}\left[z^2\right]}{\mathbb{E}\left[z^4\right] - \mathbb{E}^2\left[z^2\right]}, \tag{53}$$

$$\varphi = \frac{\mathbb{E}^2\left[z^2\right]}{\mathbb{E}\left[z^4\right] - \mathbb{E}^2\left[z^2\right]}, \tag{54}$$

where $\mathbb{E}\left[z^2\right]$ is given in (87), and $\mathbb{E}\left[z^4\right]$ is given in (88).

Proof: Please refer to Appendix F. ∎

In order to validate the accuracy of the PDF given in (51), we compare it with its exact simulated PDF, as illustrated in Fig. 2. We obtain the theoretical and Monte-Carlo simulation results by setting $N = \{2, 5, 10, 20, 30\}$, $\sigma_{h_i}^2 = \sigma_{g_i}^2 = 1$, $\mu_{h_i}^R = \mu_{g_i}^R = 2$ and $\mu_{h_i}^I = \mu_{g_i}^I = 1$. The figure clearly demonstrates a perfect alignment between the theoretical and Monte-Carlo simulation results for different values of N. Consequently, this observation verifies the preciseness of (51) for any arbitrary number of REs.

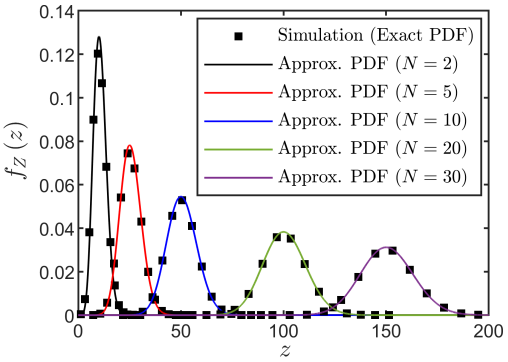

Fig. 2 Comparison of exact and approximated PDFs of z.

V. IRS-ASSISTED MULTI-ANTENNA SYSTEMS

In this section, our aim is to evaluate the BER performance of IRS-assisted wireless communication systems that utilize multiple antennas under AWGGN, and different IRS transmission schemes and fading channels. To accomplish this, we extend the analytical BER expressions derived in Section III to incorporate the scenarios of multi-antenna transceiver employing various reception and transmission diversity schemes, including EGC, MRC, EGT and MRT.

A. Multi-antenna Receiver

We first consider an IRS-assisted single-input multiple-output (SIMO) wireless communication system, where the number of receive antennas is denoted by M_r. Let $g_{i,r}$ $\forall i = 1, \ldots, N$ $\forall r = 1, \ldots, M_r$ represent the IRS-R fading channel coefficients, and similar to Section II, h_i represent the T-IRS fading channel coefficients. Moreover, two distinct cases are taken into account: (i) R employs the EGC reception diversity scheme, and (ii) R employs the MRC reception diversity scheme. For brevity, by exploiting [54] and [55], the received SNR expressions under different IRS transmission schemes given in (32), (41) and (49), can be expressed for both reception diversity schemes as

$$\gamma_{\text{EGC}} = \frac{E_b}{N_0}\zeta\left(\frac{1}{\sqrt{M_r}}\sum_{r=1}^{M_r} z_r\right)^2 . \tag{55}$$

$$\gamma_{\text{MRC}} = \frac{E_b}{N_0}\zeta\sum_{r=1}^{M_r} z_r^2 . \tag{56}$$

It should be noted that, similar to (32), (41), and (49), the following can be written for different transmission schemes: $z_r \triangleq \left|\sum_{i=1}^{N} |h_i||g_{i,r}|\right|$ for the intelligent transmission

scheme, $z_r \triangleq \left|\sum_{i=1}^{N}|h_i||g_{i,r}|e^{j\phi_i}\right|$ for transmission with imperfect phase shifts, and $z_r \triangleq \left|\sum_{i=1}^{N} h_i g_{i,r}\right|$ for the blind transmission scheme. Moreover, by exploiting the Cauchy-Schwarz inequality for the sum of squared positive variables, it can be written that $\frac{1}{L}\left(\sum_{l=1}^{L} x_l\right)^2 \leq \sum_{l=1}^{L} x_l^2 \leq \left(\sum_{l=1}^{L} x_l\right)^2$ [56], [57]. Therefore, similar to [57, Eq. (11)], the received SNR in the MRC diversity scheme can be upper-bounded as

$$\gamma_{\text{MRC}} \leq \frac{E_b}{N_0}\zeta\left(\sum_{r=1}^{M_r} z_r\right)^2. \tag{57}$$

In addition, using (55) and assuming mutually independent and identically distributed channels, the end-to-end CHF in the EGC diversity scheme is expressed as

$$\Phi_{\text{EGC}}(\omega) = \mathbb{E}\left[e^{j\omega\frac{1}{\sqrt{M_r}}\sum_{r=1}^{M_r} z_r}\right] = \left[\Phi_z\left(\frac{\omega}{\sqrt{M_r}}\right)\right]^{M_r}, \tag{58}$$

where $\Phi_z\left(\frac{\omega}{\sqrt{M_r}}\right)$ is the CHF for the case of a single-antenna system, which is provided for different IRS transmission schemes and fading channels in Section IV.

Similarly, for mutually independent and identically distributed channels, using (57), the end-to-end CHF in the MRC diversity scheme can be expressed as

$$\Phi_{\text{MRC}}(\omega) = \mathbb{E}\left[e^{j\omega\sum_{r=1}^{M_r} z_r}\right] = \left[\Phi_z(\omega)\right]^{M_r}. \tag{59}$$

B. Multi-antenna Transmitter

Now let's consider an IRS-assisted multiple-input single-output (MISO) wireless communication system, where T is equipped with M_t antennas that may employ EGT or MRT diversity schemes. Let $h_{t,i}$ $\forall t = 1,\ldots,M_t$ $\forall i = 1,\ldots,N$ represent the T-IRS fading channel coefficients, and similar to Section II, g_i represent the IRS-R fading channel coefficients. Therefore, for both transmission diversity schemes, by exploiting [11] and [55], the received SNR expressions under different IRS transmission schemes given in (32), (41) and (49), can be expressed as

$$\gamma_{\text{EGT}} = \frac{E_b}{N_0}\zeta\left(\frac{1}{\sqrt{M_t}}\sum_{t=1}^{M_t} z_t\right)^2, \tag{60}$$

$$\gamma_{\text{MRT}} = \frac{E_b}{N_0}\zeta\sum_{t=1}^{M_t} z_t^2 \leq \frac{E_b}{N_0}\zeta\left(\sum_{t=1}^{M_t} z_t\right)^2, \tag{61}$$

where $z_t \triangleq \sum_{i=1}^{N}|h_{t,i}||g_i|$ for intelligent transmission, $z_t \triangleq \left|\sum_{i=1}^{N}|h_{t,i}||g_i|e^{j\phi_i}\right|$ for transmission with imperfect phase shifts, and $z_t \triangleq \left|\sum_{i=1}^{N} h_{t,i}g_i\right|$ for blind transmission.

Therefore, similar to the EGC and MRC diversity schemes, the end-to-end CHFs for the EGT and MRT diversity schemes are respectively expressed as

$$\Phi_{\text{EGT}}(\omega) = \left[\Phi_z\left(\frac{\omega}{\sqrt{M_t}}\right)\right]^{M_t}. \tag{62}$$

$$\Phi_{\text{MRT}}(\omega) = \left[\Phi_z(\omega)\right]^{M_t}. \tag{63}$$

Finally, by substituting (58), (59), (62), and (63) into (22), and then by substituting (22) into (14), (18) and (21), the average BER of IRS-assisted multi-antenna systems in AWGGN and various modulation schemes under different reception and transmission diversity schemes is obtained.

VI. Numerical and Simulation Results

In order to numerically assess the BER performance of IRS-assisted communication systems in AWGGN and different transmission schemes and fading channels, as well as to verify the accuracy of the unified BER and CHF expressions, we provide numerical and simulation results. The simulation setup for the IRS deployment is shown in Fig. 3. In this setup, the horizontal distance between T and R is set as $D = 50$ m, the IRS-R horizontal distance is set as $d = 40$ m, the height of T is set as $H_T = 3$ m, the height of R is set as $H_R = 2$ m, and the IRS is deployed above T and R at a height of $H_I = 5$ m, where we assume that the location of IRS can be moved horizontally towards T and R. Therefore, the angle of incidence at the IRS, and the distances for the T-IRS and IRS-R links are $\psi = \arctan\left(\frac{D-d}{H_I - H_T}\right)$, $d_T = \sqrt{(D-d)^2 + (H_I - H_T)^2}$ and $d_R = \sqrt{d^2 + (H_I - H_R)^2}$, respectively. Furthermore, unless otherwise stated, the remaining required parameters are set as $G_T = G_R = 20$ dBi, $W = 1$ m, $L = 2$ m, $\eta = \{1, 2\}$, $N = \{10, 25, 30, 50\}$, and $M_t = M_r = \{1, 3\}$.

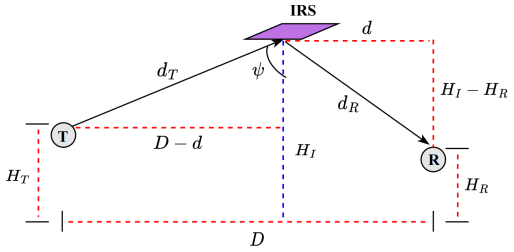

Fig. 3 Simulation setup for IRS deployment.

Fig. 4 (a) and Fig. 4 (b) show the BER performance against E_b/N_0 in intelligent transmission for BPSK, 4PAM and 64QAM modulation formats, $N = \{10, 50\}$, and double Rayleigh fading channels with $\sigma_{h_i}^2 = \sigma_{g_i}^2 = 1$ under AWGN and Laplacian noise, respectively. Similarly, Fig. 5 (a) and Fig. 5 (b) show the BER in intelligent transmission for double α-μ fading channels with $\alpha_{h_i} = \alpha_{g_i} = 1$, $\Omega_{h_i} = \Omega_{g_i} = 1$, and $\mu_{h_i} = \mu_{g_i} = 4$ under AWGN and Laplacian noise, respectively. Moreover, Fig. 6 (a) and Fig. 6 (b) respectively depict the BER under transmission with imperfect phase shifts in AWGN and Laplacian noise for BPSK and 4PAM, $q = 1$ bit, $N = \{10, 50\}$, and different fading channels. These include double Rayleigh channels with $\sigma_{h_i}^2 = \sigma_{g_i}^2 = 1$, double Rician channels with $\mu_{h_i} = \mu_{g_i} = 1$ and $\sigma_{h_i}^2 = \sigma_{g_i}^2 = 1$, and double Nakagami-$m$ channels with $\Omega_{h_i} = \Omega_{g_i} = 1$ and $m_{h_i} = m_{g_i} = 2$. In addition, Fig. 7 (a) shows the BER performance of the system with blind transmission for BPSK, 4PAM, and 64QAM modulation formats, zero-mean and non-zero mean complex Gaussian fading channels, i.e. $\mu_{h_i}^R = \mu_{g_i}^R = \{0, 1\}$, $\mu_{h_i}^I = \mu_{g_i}^I = 0$ and $\sigma_{h_i}^2 = \sigma_{g_i}^2 = 1$, and $N = \{10, 50\}$ under AWGN, while Fig. 7 (b) depicts the corresponding performance under Laplacian noise.

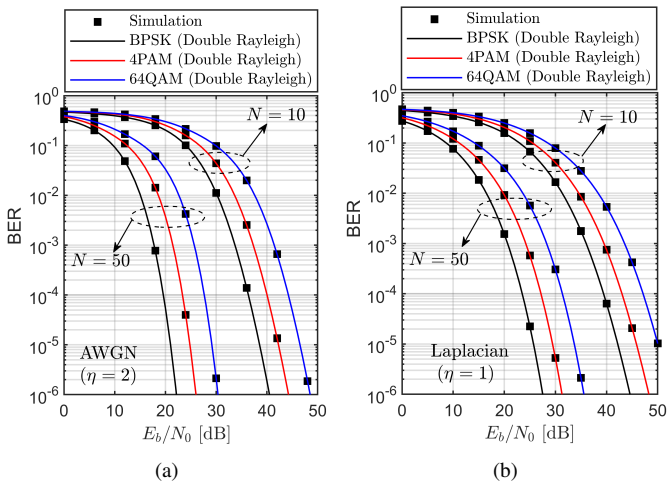

Fig. 4 BER of BPSK, 4PAM and 64QAM modulation schemes in intelligent transmission under Rayleigh fading channels for $M_t = M_r = 1$ and $N = \{10, 50\}$ (a) AWGN (b) Laplacian noise.

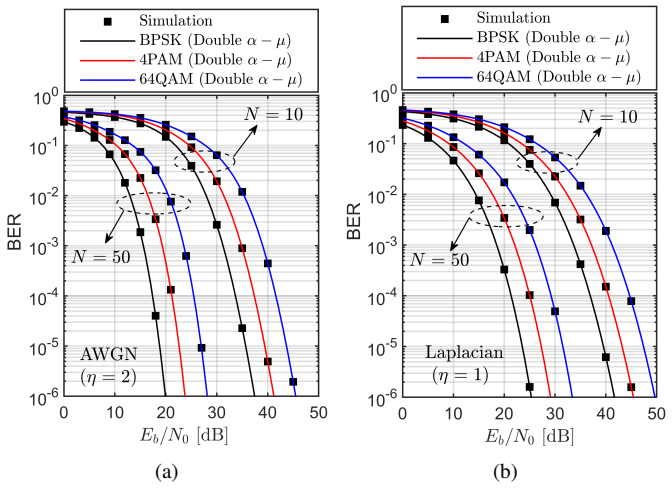

Fig. 5 BER of BPSK, 4PAM and 64QAM modulation schemes in intelligent transmission under α-μ fading channels for $M_t = M_r = 1$ and $N = \{10, 50\}$ (a) AWGN (b) Laplacian noise.

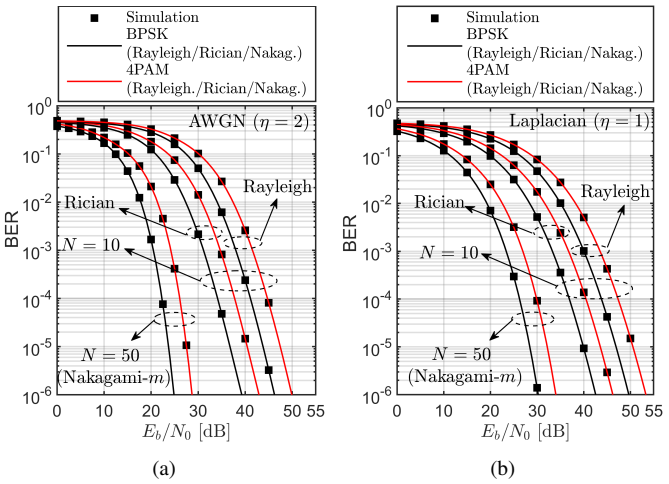

Fig. 6 BER in transmission with imperfect phase shifts under Rayleigh, Rician and Nakagami-m fading channels for $q = 1$ bit, $M_t = M_r = 1$ and $N = \{10, 50\}$ (a) AWGN (b) Laplacian noise.

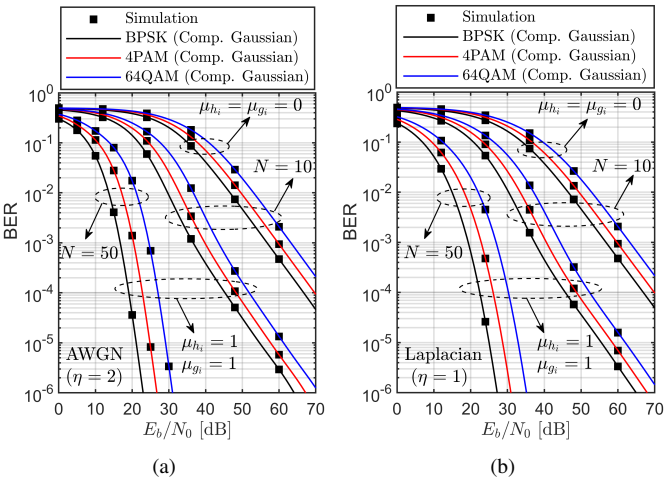

Fig. 7 BER of BPSK, 4PAM and 64QAM in blind transmission under zero/non-zero mean complex Gaussian fading channels for $M_t = M_r = 1$ and $N = \{10, 50\}$ (a) AWGN (b) Laplacian noise.

As shown in the figures, the numerical results exactly match those of the Monte-Carlo simulations, which verifies the preciseness of the BER expressions derived in Section III, for an arbitrary number of REs, different transmission schemes, different types of noise, and general fading channels. Moreover, the figures confirm the preciseness of the CHF expressions under different transmission schemes given in (35), (36), (42), (50) and (52). It can be seen from the figures that in different transmission schemes and fading channels, the system in the presence of AWGN (i.e. $\eta = 2$) achieves better BER performance compared to that of the Laplacian noise (i.e. $\eta = 1$). This observation shows that the adverse effects of noise on the received signal are more severe with lower values of the shape parameter of AWGGN. It should be noted that lower values of the shape parameter of the generalized Gaussian distributed RV or noise models that follow distributions with heavier tails imply that, in addition to the thermal noise, different sources of noise such as non-Gaussian noise arising in various practical scenarios are also taken into account, which adversely affect the BER.

In addition, in various transmission schemes, noise models and fading channels, higher orders of modulations lead to a higher BER which can be significantly improved by increasing the number of REs. For instance, as illustrated in the aforementioned figures, the BER of 4PAM and 64QAM with $N = 50$ is considerably lower compared to that of BPSK with $N = 10$. This improvement stems from each RE providing an additional indirect transmission path, resulting in significant enhancements in the received signal power.

Fig. 8 (a) compares the BER performance of an IRS-assisted multi-antenna system employing 4PAM modulation and the EGC/EGT diversity schemes under different types of IRS transmission in AWGN and Laplacian noise. The system assumes zero-mean complex Gaussian (Rayleigh) fading channels with $\{\sigma^2_{h_i}, \sigma^2_{h_{t,i}}, \sigma^2_{g_i}, \sigma^2_{g_{i,r}}\} = 1$, and sets the number of antennas as $\{M_r, M_t\} = 3$, the number of REs as $N = 50$, and the number of quantization bits as $q = 1$ bit. Meanwhile, Fig. 8 (b) compares the BER of an IRS-assisted multi-antenna system employing the MRC/MRT diversity schemes under the same system parameters. Both

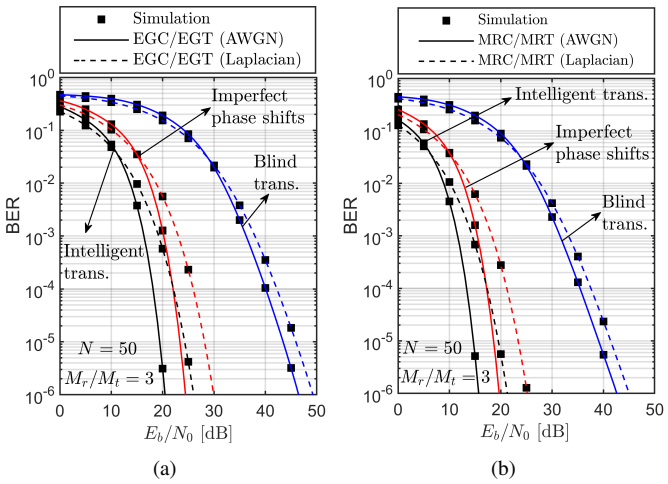

Fig. 8 Comparison of different transmission schemes for a multi-antenna IRS-assisted system under AWGN and Laplacian noise with Rayleigh fading channels, 4PAM modulation, $M_r/M_t = 3$, $N = 50$ and $q = 1$ bit (a) EGC/EGT (b) MRC/MRT.

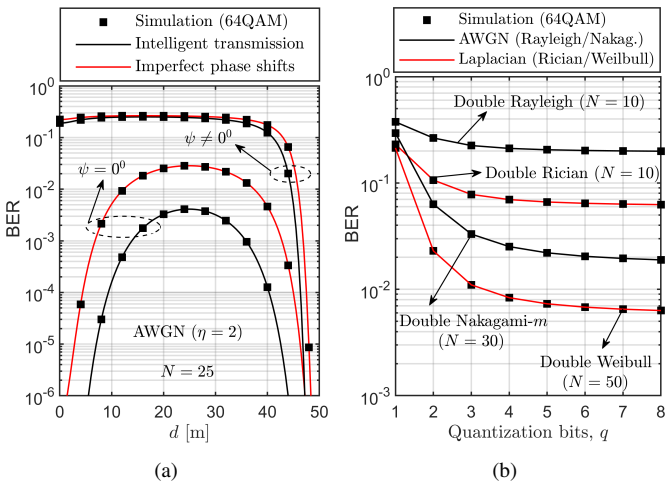

Fig. 9 BER of the system with 64QAM (a) Impacts of IRS location and angle of incidence in intelligent transmission and transmission with imperfect phase shifts in AWGN (b) Impacts of quantization bits in AWGN/Laplacian noise and different fading channels.

figures demonstrate a perfect match between the numerical and Monte-Carlo simulation results, verifying the applicability and preciseness of the unified BER expressions derived in Section III, for IRS-assisted multi-antenna systems employing different reception and transmission diversity schemes.

As shown in Fig. 8 (a) and Fig. 8 (b), the lowest BER is achieved with the intelligent transmission scheme. This is attributed to the fact that the phases of the IRS fading channels are assumed to be known at the IRS, and the REs apply phase shifts to align the T-IRS and IRS-R phases, forming strong beams towards R that result in significant improvements in the received signal. Furthermore, it is shown that the BER performance in transmission with imperfect phase shifts is better compared to that of the blind transmission scheme. This is because the phase information is partially known at the IRS and/or the IRS applies discrete quantized phase shifts with quantization errors. These imperfect phase shifts cause the IRS to partially direct the incident signals towards R, and while not maximizing the signal power, they improve the received signal.

On the other hand, under different types of noise and diversity schemes, the system with blind transmission achieves a higher BER compared to other transmission schemes as the IRS does not apply phase shifts to form beams but blindly reflects the incident signals. Moreover, under different types of IRS transmission, the system with multiple antennas employing MRC/MRT achieves an improved BER compared to that of the single-antenna and multi-antenna with EGC/EGT. However, increasing the number of active antenna elements and employing MRC/MRT increase the cost and signal processing complexity. Additionally, in the blind transmission scheme, one may assume that T can communicate with R by utilizing an ambient IRS, which can be a promising candidate for low-cost and low-data rate communications such as IoT, as it does not require excessive channel estimation overhead and computational complexity.

Fig. 9 (a) depicts the impacts of the IRS location and angle of incidence on the BER under different transmission schemes in AWGN. The system parameters considered are as follows: the number of REs is $N = 25$, the modulation format is 64QAM, $E_b/N_0 = 20$ dB, the number of phase shift quantization bits is $q = 1$, and the IRS fading channel coefficients are modeled as zero-mean complex Gaussian RVs with $\sigma^2_{h_i} = \sigma^2_{g_i} = 1$. As shown in the figure, regardless of the transmission scheme and IRS-R horizontal distance, d, a better BER performance is achieved by placing the IRS in direct sight of T, where the angle of incidence becomes $\psi = 0$. This is because $\cos(0) = 1$, and thus, according to (1), the large-scale path gain is improved, leading to improvements in the received signal power and system performance.

It is also shown that for $\psi = 0$, the BER performance is further improved by deploying the IRS close to either T or R. For example, when $\psi = 0$, the highest BER is achieved at $d = \frac{D}{2} = 25$ m, which means that the IRS is deployed between T and R with equal T-IRS and IRS-R horizontal distances, whereas it is minimized by deploying the IRS at either $d << D$ m or $d \approx D$ m. On the other hand, when the angle of incidence is $\psi = \arctan\left(\frac{D-d}{H_I - H_T}\right) \neq 0$, the best BER performance is achieved when the IRS is deployed close to T. For example, as shown in the figure, for $\psi \neq 0$ and different transmission schemes, the BER is significantly improved by placing the IRS at $d \approx D \approx 50$ m. As a result, regardless of the angle of incidence, by placing the IRS close to T, the BER is significantly improved.

Fig. 9 (b) illustrates the impacts of the number of quantization bits on the BER of 64QAM modulation in AWGN and Laplacian noise under different fading channels with $M_t = M_r = 1$ and $E_b/N_0 = 25$ dB. The system parameters for different fading channels are set as follows: for Rayleigh fading channels, we set $N = 10$, $\sigma^2_{h_i} = \sigma^2_{g_i} = 1$, and $\eta = 2$; for Rician fading channels, we set $N = 10$, $\mu_{h_i} = \mu_{g_i} = 1$, $\sigma^2_{h_i} = \sigma^2_{g_i} = 1$, and $\eta = 1$; for Nakagami-m fading channels, we set $N = 30$, $\Omega_{h_i} = \Omega_{g_i} = 1$, $m_{h_i} = m_{g_i} = 2$, and $\eta = 2$; and for Weibull fading channels, we set $N = 50$, $\Omega_{h_i} = \Omega_{g_i} = 1$, $\alpha_{h_i} = \alpha_{g_i} = 2$, and $\eta = 1$. From the figure, it is evident that under different fading channels and noise models, setting the number of quantization bits to

$q \geq 4$ significantly improves the BER. This improvement can be attributed to the fact that increasing the number of quantization bits leads to a higher number of phase shift quantization levels. As a result, the precision of the applied phase shifts increases, leading to further enhancements in the received SNR. However, this comes at the expense of increased hardware complexity and cost.

VII. Conclusion

This paper studied the BER performance of IRS-assisted systems over generalized Gaussian noise and fading channels in different transmission schemes. New expressions for the BER analysis of various modulation formats were derived. Moreover, accurate expressions for the characteristic functions of different channels such as double Rayleigh, double Rician, double Nakagami-m, double $\alpha-\mu$, and the sum of zero/non-zero mean double complex Gaussian random variables were extracted. It was shown that the BER expressions are readily applicable to multi-antenna systems employing different reception and transmission diversity schemes. Moreover, it was observed that the IRS with full phase information achieves the lowest BER compared to the cases when the IRS has no phase information and partial phase information with discrete phase shifts. However, it was demonstrated that setting the number of phase shift quantization bits to 4 or more significantly improves the BER in transmission with imperfect phase shifts. Finally, it was shown that by deploying the IRS in front of the transmitter and close to either the transmitter or receiver, the BER is significantly improved.

Appendix A
Proof of Lemma 1

According to the convolution theorem for the Fourier cosine transform, the average of an absolutely integrable function, $g(x)$, with a PDF of $f_X(x)$ can be obtained as [54, Eq. (3)]

$$\mathbb{E}\left[g(x)\right] = \frac{2}{\pi}\int_0^\infty \mathcal{F}_c(\omega)\,\mathrm{Re}\,\Phi_x\left(\omega\right)\mathrm{d}\omega, \tag{64}$$

where $\mathcal{F}_c(\omega)$ is the Fourier cosine transform of $g(x)$, and $\mathrm{Re}\,\Phi_x\left(\omega\right)$ is the real part of the CHF of x.

Therefore, in order to derive the average of the generalized Gaussian Q-function, by exploiting (64), it can be written that

$$\begin{aligned}\mathcal{E} &= \mathbb{E}\left[Q_\eta\left(\mathcal{B}\sqrt{\frac{E_b\zeta}{N_0}}z\right)\right]\\ &= \frac{2}{\pi}\int_0^\infty \mathcal{F}_c(\omega)\,\mathrm{Re}\,\Phi_z\left(\omega\right)\mathrm{d}\omega,\end{aligned} \tag{65}$$

where $\mathcal{F}_c(\omega)$ is the Fourier cosine transform of the generalized Gaussian Q-function, and $\Phi_z\left(\omega\right)$ is the CHF of the sum of RVs, $z \triangleq \left|\sum_{i=1}^N h_i \mathrm{e}^{j\theta_i} g_i\right|$. Furthermore, $\mathcal{F}_c(\omega)$ and $\Phi_z\left(\omega\right)$ are respectively expressed as

$$\mathcal{F}_c(\omega) = \int_0^\infty \cos(\omega z) Q_\eta\left(\mathcal{B}\sqrt{\frac{E_b\zeta}{N_0}}z\right)\,\mathrm{d}z. \tag{66}$$

$$\Phi_z(\omega) = \int_0^\infty e^{j\omega z} f_Z(z)\mathrm{d}z. \tag{67}$$

In order to derive $\mathcal{F}_c(\omega)$, by exploiting (9) and [24, Eq. (A.4)], the generalized Gaussian Q-function can be written in terms of the upper incomplete gamma function as

$$Q_\eta\left(\mathcal{B}\sqrt{\frac{E_b\zeta}{N_0}}z\right) = \frac{1}{2\Gamma\left(\frac{1}{\eta}\right)}\Gamma\left(\frac{1}{\eta}, \left(\mathcal{B}\sqrt{\frac{\vartheta_0^2 E_b\zeta}{N_0}}z\right)^\eta\right). \tag{68}$$

Furthermore, by exploiting [41, Eq. (07.34.03.0613.01)], (68) can be written in a more convenient form as

$$Q_\eta\left(\mathcal{B}\sqrt{\frac{E_b\zeta}{N_0}}z\right) = \frac{G_{1,2}^{2,0}\left[\left(\mathcal{B}\sqrt{\frac{\vartheta_0^2 E_b\zeta}{N_0}}z\right)^\eta \middle| \begin{matrix}1\\ 0, \frac{1}{\eta}\end{matrix}\right]}{2\Gamma(1/\eta)}. \tag{69}$$

Using (66) and (69), $\mathcal{F}_c(\omega)$ in AWGGN is derived as

$$\mathcal{F}_c(\omega) = \int_0^\infty \frac{\cos(\omega z)}{2\Gamma(1/\eta)} G_{1,2}^{2,0}\left[\left(\mathcal{B}\sqrt{\frac{\vartheta_0^2 E_b\zeta}{N_0}}z\right)^\eta \middle| \begin{matrix}1\\ 0, \frac{1}{\eta}\end{matrix}\right]\mathrm{d}z. \tag{70}$$

By applying [41, Eq. (07.34.21.0090.01)], the integral of (70) is evaluated. Finally, by substituting (70) into (65), and after some algebraic manipulations, the average of the generalized Gaussian Q-function given in (22) is obtained. ■

Appendix B
Proof of Corollary 2

In order to derive a further simplified expression for the exact BER analysis in Laplacian noise, by setting $\eta = 1$ in (69), it can be written that

$$Q_1\left(\mathcal{B}\sqrt{\frac{E_b\zeta}{N_0}}z\right) = \frac{1}{2}\, G_{1,2}^{2,0}\left[2\mathcal{B}\sqrt{\frac{E_b\zeta}{N_0}}z \middle| \begin{matrix}1\\ 0, 1\end{matrix}\right]. \tag{71}$$

By applying [41, Eq. (07.34.03.0613.01)] and [26, Eq. (8.356.2)], (71) can be explicitly written as

$$\begin{aligned}Q_1\left(\mathcal{B}\sqrt{\frac{E_b\zeta}{N_0}}z\right) &= \frac{1}{2}\Gamma\left(1, 2\mathcal{B}\sqrt{\frac{E_b\zeta}{N_0}}z\right)\\ &= \frac{1}{2}\,\exp\left(-2\mathcal{B}\sqrt{\frac{E_b\zeta}{N_0}}z\right).\end{aligned} \tag{72}$$

By exploiting (66), the Fourier cosine transform of (72) is written as

$$\mathcal{F}_c(\omega) = \frac{1}{2}\int_0^\infty \cos(\omega z)\,\exp\left(-\mathcal{B}\sqrt{\frac{2E_b\zeta}{N_0}}z\right)\mathrm{d}z. \tag{73}$$

By applying [26, Eq. (3.944.6)], the integral of (73) is evaluated as

$$\begin{aligned}\mathcal{F}_c(\omega) &= \frac{1}{2\sqrt{\left(\omega^2 + 2\mathcal{B}^2\frac{E_b\zeta}{N_0}\right)}}\cos\left(\arctan\left(\frac{\omega}{\mathcal{B}\sqrt{\frac{2E_b\zeta}{N_0}}}\right)\right)\\ &= \frac{\sqrt{\mathcal{B}^2\zeta\frac{E_b}{N_0}}}{\omega^2 + 4\mathcal{B}^2\zeta\frac{E_b}{N_0}},\end{aligned} \tag{74}$$

where the last step is obtained by applying the identity $\cos\left(\arctan(\alpha)\right) = \frac{1}{\sqrt{1+\alpha^2}}$.

Finally, by substituting (74) into (65), the expression given in (30) is obtained. ■

APPENDIX C
PROOF OF LEMMA 2

Let's assume that $z_i = |h_i||g_i|$ is a double Rayleigh RV, where $|h_i|$ and $|g_i|$ can be non-identical, and thus by exploiting [58, Eq. (8)], its exact PDF is written as

$$f_{Z_i}(z_i) = \frac{2}{\sigma_{h_i}\sigma_{g_i}} G_{0,2}^{2,0}\left[\frac{z_i^2}{\sigma_{h_i}^2\sigma_{g_i}^2}\,\middle|\,\begin{matrix}-\\ \frac{1}{2},\frac{1}{2}\end{matrix}\right]. \tag{75}$$

By applying the identity provided in [41, Eq. (07.34.03.0605.01)], we can express (75) in an equivalent form as follows.

$$f_{Z_i}(z_i) = \frac{4z_i}{\sigma_{h_i}^2\sigma_{g_i}^2} K_0\left(\frac{2z_i}{\sigma_{h_i}\sigma_{g_i}}\right). \tag{76}$$

Therefore, the CHF of z_i is derived as

$$\begin{aligned}\Phi_{z_i}(\omega) =& \frac{4}{\sigma_{h_i}^2\sigma_{g_i}^2}\left(\int_0^\infty \cos(\omega z_i) z_i K_0\left(\frac{2z_i}{\sigma_{h_i}\sigma_{g_i}}\right)\mathrm{d}z_i\right.\\ &\left. + j\int_0^\infty \sin(\omega z_i) z_i K_0\left(\frac{2z_i}{\sigma_{h_i}\sigma_{g_i}}\right)\mathrm{d}z_i\right).\end{aligned} \tag{77}$$

By applying [26, Eq. (6.699.4)] and [26, Eq. (6.691)], the integrals of (77) are respectively evaluated, and after some algebraic manipulations, the CHF expression given in (35) is obtained. ■

APPENDIX D
PROOF OF LEMMA 3

We assume that $z_i = |h_i||g_i|$ is the product of two i.n.id $\alpha-\mu$ RVs, where its exact PDF is written as [42, Eq. (11)]

$$\begin{aligned}f_{Z_i}(z_i) =& \frac{z_i^{-1}}{\Gamma(\mu_{h_i})\Gamma(\mu_{g_i})}\\ &\times H_{0,2}^{2,0}\left[\frac{\mu_{h_i}^{\frac{1}{\alpha_{h_i}}}\mu_{g_i}^{\frac{1}{\alpha_{g_i}}} z_i}{\Omega_{h_i}^{\frac{1}{\alpha_{h_i}}}\Omega_{g_i}^{\frac{1}{\alpha_{g_i}}}}\,\middle|\,\begin{matrix}-\\ \left(\mu_{h_i},\frac{1}{\alpha_{h_i}}\right),\left(\mu_{g_i},\frac{1}{\alpha_{g_i}}\right)\end{matrix}\right].\end{aligned} \tag{78}$$

By leveraging (78), the CHF of double $\alpha-\mu$ distribution is derived as

$$\Phi_{z_i}(\omega) = \mathcal{I}_1 + j\mathcal{I}_2, \tag{79}$$

where

$$\begin{aligned}\mathcal{I}_1 =& \frac{1}{\Gamma(\mu_{h_i})\Gamma(\mu_{g_i})}\int_0^\infty z_i^{-1}\cos(\omega z_i)\\ &\times H_{0,2}^{2,0}\left[\frac{\mu_{h_i}^{\frac{1}{\alpha_{h_i}}}\mu_{g_i}^{\frac{1}{\alpha_{g_i}}} z_i}{\Omega_{h_i}^{\frac{1}{\alpha_{h_i}}}\Omega_{g_i}^{\frac{1}{\alpha_{g_i}}}}\,\middle|\,\begin{matrix}-\\ \left(\mu_{h_i},\frac{1}{\alpha_{h_i}}\right),\left(\mu_{g_i},\frac{1}{\alpha_{g_i}}\right)\end{matrix}\right]\mathrm{d}z_i.\end{aligned} \tag{80}$$

$$\begin{aligned}\mathcal{I}_2 =& \frac{1}{\Gamma(\mu_{h_i})\Gamma(\mu_{g_i})}\int_0^\infty z_i^{-1}\sin(\omega z_i)\\ &\times H_{0,2}^{2,0}\left[\frac{\mu_{h_i}^{\frac{1}{\alpha_{h_i}}}\mu_{g_i}^{\frac{1}{\alpha_{g_i}}} z_i}{\Omega_{h_i}^{\frac{1}{\alpha_{h_i}}}\Omega_{g_i}^{\frac{1}{\alpha_{g_i}}}}\,\middle|\,\begin{matrix}-\\ \left(\mu_{h_i},\frac{1}{\alpha_{h_i}}\right),\left(\mu_{g_i},\frac{1}{\alpha_{g_i}}\right)\end{matrix}\right]\mathrm{d}z_i.\end{aligned} \tag{81}$$

The integrals of $\mathcal{I}_1$ and $\mathcal{I}_2$ are evaluated by [27, Eq. (2.50)] and [27, Eq. (2.49)], respectively. By substituting them into (79), the CHF expression given in (36) is obtained. ■

APPENDIX E
PROOF OF LEMMA 4

We assume that $z_i = h_i g_i$ is a zero-mean double complex Gaussian RV, where h_i and g_i can be non-identically distributed RVs. Therefore, using [59, Eq. (17)], the exact PDF of $z = \left|\sum_{i=1}^N z_i\right|$ is written as

$$f_Z(z) = \frac{4z^N}{\Gamma(N)\left(\sigma_{h_i}\sigma_{g_i}\right)^{N+1}} K_{N-1}\left(\frac{2z}{\sigma_{h_i}\sigma_{g_i}}\right). \tag{82}$$

Using (82), the CHF of z is derived as

$$\begin{aligned}\Phi_z(\omega) =& \frac{4}{\Gamma(N)\left(\sigma_{h_i}\sigma_{g_i}\right)^{N+1}}\\ &\times\left[\underbrace{\int_0^\infty z^N\cos(\omega z) K_{N-1}\left(\frac{2z}{\sigma_{h_i}\sigma_{g_i}}\right)\mathrm{d}z}_{\mathcal{K}_1}\right.\\ &\left.+ j\underbrace{\int_0^\infty z^N\sin(\omega z) K_{N-1}\left(\frac{2z}{\sigma_{h_i}\sigma_{g_i}}\right)\mathrm{d}z}_{\mathcal{K}_2}\right].\end{aligned} \tag{83}$$

The integrals $\mathcal{K}_1$ and $\mathcal{K}_2$ are respectively evaluated through [26, Eq. (6.699.4)] and [26, Eq. (6.699.3)], and after some algebraic manipulations, (50) is obtained. ■

APPENDIX F
PROOF OF LEMMA 5

In order to derive (51) and (52), we can rewrite that $h_i = h_i^R + jh_i^I$ and $g_i = g_i^R + jg_i^I$, where $h_i^R \sim \mathcal{N}\left(\mu_{h_i}^R, \sigma_{h_i}^2/2\right)$, $h_i^I \sim \mathcal{N}\left(\mu_{h_i}^I, \sigma_{h_i}^2/2\right)$, $g_i^R \sim \mathcal{N}\left(\mu_{g_i}^R, \sigma_{g_i}^2/2\right)$ and $g_i^I \sim \mathcal{N}\left(\mu_{g_i}^I, \sigma_{g_i}^2/2\right)$. Therefore, z^2 can be written as

$$\begin{aligned}z^2 &= \left|\sum_{i=1}^N \left(h_i^R + jh_i^I\right)\left(g_i^R + jg_i^I\right)\right|^2\\ &= \left(\sum_{i=1}^N\left(h_i^R g_i^R - h_i^I g_i^I\right)\right)^2 + \left(\sum_{i=1}^N\left(h_i^R g_i^I + h_i^I g_i^R\right)\right)^2\\ &\triangleq z_R^2 + z_I^2.\end{aligned} \tag{84}$$

From (84), $z^2 = z_R^2 + z_I^2$ is the sum of positive RVs, and thus by virtue of [49, Sec. (2.2.2)], z_R and z_I can be tightly approximated by the first branch of the Laguerre expansion which is equivalent to gamma distribution. Therefore, z_R^2 and z_I^2 are modelled by the generalized gamma distribution [60]. In addition, z^2 is the sum of two generalized gamma distributed RVs, where its PDF is expressed as [60, Eq. (12)]

$$f_{z^2}(x) = \frac{\Psi}{\Gamma(\varphi)} H_{0,1}^{1,0}\left[\Psi x\,\middle|\,\begin{matrix}-\\ (\varphi-1,1)\end{matrix}\right], \tag{85}$$

where Ψ and φ are written as (53) and (54), respectively.

In order to derive the CHF of z, we first need to derive its PDF, and thus by exploiting [27, Eq. (1.2) and Eq. (1.112)], and by applying $f_Z(z) = 2z f_{z^2}\left(z^2\right)$, the PDF expression

given in (51) is obtained. Furthermore, by leveraging (51), the CHF of z is derived as

$$\Phi_z(\omega) = \frac{2\Psi}{\Gamma(\varphi)} \int_0^\infty z \cos(\omega z)\, G_{0,1}^{1,0}\left[\Psi z^2 \,\middle|\, \begin{matrix} - \\ \varphi - 1 \end{matrix}\right] \mathrm{d}z + j\frac{2\Psi}{\Gamma(\varphi)} \int_0^\infty z \sin(\omega z)\, G_{0,1}^{1,0}\left[\Psi z^2 \,\middle|\, \begin{matrix} - \\ \varphi - 1 \end{matrix}\right] \mathrm{d}z. \tag{86}$$

The integrals of (86) are respectively evaluated through [41, Eq. (07.34.21.0090.01)] and [41, Eq. (07.34.21.0089.01)], and by applying [26, Eq. (9.31.5)], the CHF expression given in (52) is obtained. In addition, to obtain Ψ and φ given (53) and (54), we need to derive $\mathbb{E}\left[z^2\right]$ and $\mathbb{E}\left[z^4\right]$ as

$$\mathbb{E}\left[z^2\right] = \mathbb{E}\left[z_R^2\right] + \mathbb{E}\left[z_I^2\right], \tag{87}$$

$$\begin{aligned}\mathbb{E}\left[z^4\right] &= \mathbb{E}\left[\left(z_R^2 + z_I^2\right)^2\right] \\ &= \mathbb{E}\left[z_R^4\right] + \mathbb{E}\left[z_I^4\right] + 2\mathbb{E}\left[z_R^2\right]\mathbb{E}\left[z_I^2\right],\end{aligned} \tag{88}$$

where $\mathbb{E}\left[z_R^2\right] = \mathbb{V}\left[z_R\right] + \mathbb{E}^2\left[z_R\right]$, $\mathbb{E}\left[z_I^2\right] = \mathbb{V}\left[z_I\right] + \mathbb{E}^2\left[z_I\right]$, $\mathbb{E}\left[z_R^4\right] = \mathbb{E}^4\left[z_R\right] + 6\mathbb{E}^2\left[z_R\right]\mathbb{V}\left[z_R\right] + 3\mathbb{V}^2\left[z_R\right]$ and $\mathbb{E}\left[z_I^4\right] = \mathbb{E}^4\left[z_I\right] + 6\mathbb{E}^2\left[z_I\right]\mathbb{V}\left[z_I\right] + 3\mathbb{V}^2\left[z_I\right]$.

Furthermore, assuming identically distributed channels, the mean and variance of z_R and z_I are derived as follows.

$$\begin{aligned}\mathbb{E}\left[z_R\right] &= \mathbb{E}\left[\sum_{i=1}^{N}\left(h_i^R g_i^R - h_i^I g_i^I\right)\right] \\ &= N\left(\mu_{h_i}^R \mu_{g_i}^R - \mu_{h_i}^I \mu_{g_i}^I\right).\end{aligned} \tag{89}$$

$$\begin{aligned}\mathbb{E}\left[z_I\right] &= \mathbb{E}\left[\sum_{i=1}^{N}\left(h_i^R g_i^I + h_i^I g_i^R\right)\right] \\ &= N\left(\mu_{h_i}^R \mu_{g_i}^I + \mu_{h_i}^I \mu_{g_i}^R\right).\end{aligned} \tag{90}$$

$$\begin{aligned}\mathbb{V}\left[z_R\right] &= \mathbb{V}\left[z_I\right] \\ &= N\left\{\frac{\sigma_{h_i}^2 \sigma_{g_i}^2}{2} + \frac{\sigma_{h_i}^2}{2}\left[\left(\mu_{g_i}^R\right)^2 + \left(\mu_{g_i}^I\right)^2\right] + \frac{\sigma_{g_i}^2}{2}\left[\left(\mu_{h_i}^R\right)^2 + \left(\mu_{h_i}^I\right)^2\right]\right\}.\end{aligned} \tag{91}$$

Finally, we substitute the corresponding mean and variance terms into (87) and (88). We then substitute them into (53) and (54) to obtain Ψ and φ, which concludes the proof. ■

REFERENCES

[1] S. Gong, X. Lu, D. T. Hoang, D. Niyato, L. Shu, D. I. Kim, and Y.-C. Liang, "Toward smart wireless communications via intelligent reflecting surfaces: A contemporary survey," *IEEE Commun. Surveys Tuts.*, vol. 22, no. 4, pp. 2283–2314, 4th Quart. 2020.

[2] Y. Liu, X. Liu, X. Mu, T. Hou, J. Xu, M. Di Renzo, and N. Al-Dhahir, "Reconfigurable intelligent surfaces: Principles and opportunities," *IEEE Commun. Surveys Tuts.*, vol. 23, no. 3, pp. 1546–1577, 3rd Quart. 2021.

[3] L. Yang, P. Li, F. Meng, and S. Yu, "Performance analysis of RIS-assisted UAV communication systems," *IEEE Trans. Veh. Technol.*, vol. 71, no. 8, pp. 9078–9082, Aug. 2022.

[4] E. Basar, M. Di Renzo, J. De Rosny, M. Debbah, M.-S. Alouini, and R. Zhang, "Wireless communications through reconfigurable intelligent surfaces," *IEEE Access*, vol. 7, pp. 116 753–116 773, Aug. 2019.

[5] I. Yildirim, A. Uyrus, and E. Basar, "Modeling and analysis of reconfigurable intelligent surfaces for indoor and outdoor applications in future wireless networks," *IEEE Trans. Commun.*, vol. 69, no. 2, pp. 1290–1301, Feb. 2021.

[6] A. Mahmoud, S. Muhaidat, P. C. Sofotasios, I. Abualhaol, O. A. Dobre, and H. Yanikomeroglu, "Intelligent reflecting surfaces assisted UAV communications for IoT networks: Performance analysis," *IEEE Trans. Green Commun. and Net.*, vol. 5, no. 3, pp. 1029–1040, Sep. 2021.

[7] P. K. Sharma and P. Garg, "Intelligent reflecting surfaces to achieve the full-duplex wireless communication," *IEEE Commun. Lett.*, vol. 25, no. 2, pp. 622–626, Feb. 2021.

[8] D. Kudathanthirige, D. Gunasinghe, and G. Amarasuriya, "Performance analysis of intelligent reflective surfaces for wireless communication," in *Proc. IEEE Int. Conf. Commun. (ICC)*, Dublin, Ireland, Jun. 2020, pp. 1–6.

[9] M. Aldababsa, A. M. Salhab, A. A. Nasir, M. H. Samuh, and D. B. da Costa, "Multiple RISs-aided networks: Performance analysis and optimization," *IEEE Trans. Veh. Technol.*, vol. 72, no. 6, pp. 7545–7559, Jun. 2023.

[10] G. R. d. L. Tejerina, C. R. N. da Silva, R. A. A. de Souza, and M. D. Yacoub, "On the extended η-μ model: New results and applications to IRS-aided systems," *IEEE Trans. Veh. Technol.*, vol. 72, no. 4, pp. 4133–4142, Apr. 2023.

[11] A. M. Tota Khel and K. A. Hamdi, "Effects of hardware impairments on IRS-enabled MISO wireless communication systems," *IEEE Commun. Lett.*, vol. 26, no. 2, pp. 259–263, Feb. 2022.

[12] F. A. P. de Figueiredo, M. S. P. Facina, R. C. Ferreira, Y. Ai, R. Ruby, Q.-V. Pham, and G. Fraidenraich, "Large intelligent surfaces with discrete set of phase-shifts communicating through double-Rayleigh fading channels," *IEEE Access*, vol. 9, pp. 20 768–20 787, Jan. 2021.

[13] A. Al-Dweik, A. Siddig, A. Al-Rimawi, Y. Iraqi, A. Pandey, and J.-P. Giacalone, "On the performance of IRS-assisted communications with joint phase estimation errors and discrete phase control," *TechRxiv preprint. https://doi.org/10.36227/techrxiv.22100930.v1*, Feb. 2023.

[14] M.-A. Badiu and J. P. Coon, "Communication through a large reflecting surface with phase errors," *IEEE Wireless Commun. Lett.*, vol. 9, no. 2, pp. 184–188, Feb. 2020.

[15] W. Zhao, G. Wang, S. Atapattu, T. A. Tsiftsis, and C. Tellambura, "Is backscatter link stronger than direct link in reconfigurable intelligent surface-assisted system?" *IEEE Commun. Lett.*, vol. 24, no. 6, pp. 1342–1346, Jun. 2020.

[16] E. Basar, "Transmission through large intelligent surfaces: A new frontier in wireless communications," in *Proc. Eur. Conf. Netw. Commun. (EuCNC)*, Valencia, Spain, Jun. 2019, pp. 112–117.

[17] S. Sharma, K. Deka, and V. Bhatia, "Intelligent reflecting surface-aided downlink SCMA," *IEEE Syst. J*, vol. 17, no. 2, pp. 3204–3211, Jun. 2023.

[18] S. A. Tegos, D. Tyrovolas, P. D. Diamantoulakis, C. K. Liaskos, and G. K. Karagiannidis, "On the distribution of the sum of double-Nakagami-m random vectors and application in randomly reconfigurable surfaces," *IEEE Trans. Veh. Technol.*, vol. 71, no. 7, pp. 7297–7307, Jul. 2022.

[19] L. Mohjazi, L. Bariah, S. Muhaidat, and M. A. Imran, "Performance of reconfigurable intelligent surfaces in the presence of generalized Gaussian noise," *IEEE Commun. Lett.*, vol. 26, no. 4, pp. 773–777, Apr. 2022.

[20] N. Pillay and H. Xu, "Error performance analysis of access point-based reconfigurable intelligent surfaces in the presence of Gaussian-plus-Laplacian additive noise," *IEEE Access*, vol. 9, pp. 158 287–158 296, Nov. 2021.

[21] U. Ashraf and G. R. Begh, "Effect of Impulsive noise on IRS-aided communication systems," *IEEE Trans. Veh. Technol.*, vol. 72, no. 1, pp. 648–653, Jan. 2023.

[22] F. Yilmaz, "Mcleish distribution: Performance of digital communications over additive white Mcleish noise (AWMN) channels," *IEEE Access*, vol. 8, pp. 19 133–19 195, Jan. 2020.

[23] L. Bariah, S. Muhaidat, P. C. Sofotasios, S. Gurugopinath, W. Hamouda, and H. Yanikomeroglu, "Non-orthogonal multiple access in the presence of additive generalized Gaussian noise," *IEEE Commun. Lett.*, vol. 24, no. 10, pp. 2137–2141, Oct. 2020.

[24] H. Soury, F. Yilmaz, and M.-S. Alouini, "Average bit error probability of binary coherent signaling over generalized fading channels subject to additive generalized Gaussian noise," *IEEE Commun. Lett.*, vol. 16, no. 6, pp. 785–788, Jun. 2012.

[25] ——, "Error rates of M-PAM and M-QAM in generalized fading and generalized Gaussian noise environments," *IEEE Commun. Lett.*, vol. 17, no. 10, pp. 1932–1935, Oct. 2013.

[26] I. S. Gradshteyn and I. M. Ryzhik, *Table of Integrals, Series, and Products*, 8th ed. Oxford, UK: Academic Press: Elsevier, 2014.
[27] A. M. Mathai, R. K. Saxena, and H. J. Haubold, *The H-Function: Theory and Applications*. New York, NY, USA: Springer, 2010.
[28] O. Ozdogan, E. Bjornson, and E. G. Larsson, "Intelligent reflecting surfaces: Physics, propagation, and pathloss modeling," *IEEE Wireless Commun. Lett.*, vol. 9, no. 5, pp. 581–585, May 2020.
[29] T. Wang, M.-A. Badiu, G. Chen, and J. P. Coon, "Outage probability analysis of RIS-assisted wireless networks with Von Mises phase errors," *IEEE Wireless Commun. Lett.*, vol. 10, no. 12, pp. 2737–2741, Dec. 2021.
[30] J. Zhu, Y. Huang, J. Wang, K. Navaie, W. Huang, and Z. Ding, "On the position optimization of IRS," *IEEE Internet Things J.*, vol. 9, no. 14, pp. 11 712–11 724, Jul. 2022.
[31] W. Tang, M. Z. Chen, X. Chen, J. Y. Dai, Y. Han, M. Di Renzo, Y. Zeng, S. Jin, Q. Cheng, and T. J. Cui, "Wireless communications with reconfigurable intelligent surface: Path loss modeling and experimental measurement," *IEEE Trans. Wireless Commun.*, vol. 20, no. 1, pp. 421–439, Jan. 2021.
[32] X. Yue and Y. Liu, "Performance analysis of intelligent reflecting surface assisted NOMA networks," *IEEE Trans. Wireless Commun.*, vol. 21, no. 4, pp. 2623–2636, Apr. 2022.
[33] Z. Zhang, Q. Sun, J. Zhang, D. W. K. Ng, and B. Ai, "Ergodic capacity of intelligent omni-surface-aided communication systems with phase quantization errors and outdated CSI," *IEEE Syst. J.*, vol. 17, no. 2, pp. 1889–1898, Jun. 2023.
[34] K. Cho and D. Yoon, "On the general BER expression of one- and two-dimensional amplitude modulations," *IEEE Trans. Commun.*, vol. 50, no. 7, pp. 1074–1080, Jul. 2002.
[35] M. Abramowitz and I. A. Stegun, *Handbook of Mathematical Functions with Formulas, Graphs, and Mathematical Tables*, 10th ed. New York, NY, USA: Dover, 1972.
[36] J. Li, X.-D. Zhang, Q. Gao, Y. Luo, and D. Gu, "Exact BEP analysis for coherent M-ary PAM and QAM over AWGN and Rayleigh fading channels," in *Proc. IEEE Veh. Technol. Conf. (VTC)*, Marina Bay, Singapore, May 2008, pp. 390–394.
[37] M. K. Simon, S. H. Hinedid, and W. C. Lindsey, *Digital Communication Techniques: Signal Design And Detection*. Englewood Cliffs, NJ, USA: Prentice Hall, 1995.
[38] J. G. Proakis and M. Salehi, *Digital Communications*, 5th ed. New York, NY, USA: McGraw-Hill, 2008.
[39] A. Goldsmith, *Wireless Communications*. Cambridge, UK: Cambridge Univ. Press, 2005.
[40] J. Lu, K. Letaief, J.-I. Chuang, and M. Liou, "M-PSK and M-QAM BER computation using signal-space concepts," *IEEE Trans. Commun.*, vol. 47, no. 2, pp. 181–184, Feb. 1999.
[41] Wolfram Research. "*The Wolfram Functions Site: Meijer G-function*," 2001. [Online]. Available: https://functions.wolfram.com/PDF/MeijerG.pdf
[42] O. R. Durgada, V. K. Chapala, and S. Zafaruddin, "RIS-THz wireless communication with random phase noise and misaligned transceiver," *arXiv preprint arXiv:2211.08690*, Nov. 2022.
[43] A. M. Magableh and M. M. Matalgah, "Moment generating function of the generalized $\alpha - \mu$ distribution with applications," *IEEE Commun. Lett.*, vol. 13, no. 6, pp. 411–413, Jun. 2009.
[44] L. Kong, Y. Ai, S. Chatzinotas, and B. Ottersten, "Effective rate evaluation of RIS-assisted communications using the sums of cascaded $\alpha-\mu$ random variates," *IEEE Access*, vol. 9, pp. 5832–5844, Jan. 2021.
[45] A. M. Tota Khel and K. A. Hamdi, "Secrecy capacity of IRS-assisted terahertz wireless communications with pointing errors," *IEEE Commun. Lett.*, vol. 27, no. 4, pp. 1090–1094, Apr. 2023.
[46] H. Zhang, B. Di, L. Song, and Z. Han, "Reconfigurable intelligent surfaces assisted communications with limited phase shifts: How many phase shifts are enough?" *IEEE Trans. Veh. Technol.*, vol. 69, no. 4, pp. 4498–4502, Apr. 2020.
[47] Q. Wu and R. Zhang, "Beamforming optimization for wireless network aided by intelligent reflecting surface with discrete phase shifts," *IEEE Trans. Commun.*, vol. 68, no. 3, pp. 1838–1851, Mar. 2020.
[48] S. Kim, H. Lee, J. Cha, S.-J. Kim, J. Park, and J. Choi, "Practical channel estimation and phase shift design for intelligent reflecting surface empowered MIMO systems," *IEEE Trans. Wireless Commun.*, vol. 21, no. 8, pp. 6226–6241, Aug. 2022.
[49] S. Primak, V. Kontorovich, and V. Lyandres, *Stochastic Methods and Their Applications to Communications: Stochastic Differential Equations Approach*. Chichester, U.K.: Wiley, 2004.
[50] Z. Zhakipov, K. M. Rabie, X. Li, and G. Nauryzbayev, "Accurate approximation to channel distributions of cascaded RIS-aided systems with phase errors over Nakagami-m channels," *IEEE Wireless Commun. Lett.*, vol. 12, no. 5, pp. 922–926, May 2023.
[51] A. M. Tota Khel and K. A. Hamdi, "Performance analysis of IRS-assisted full-duplex wireless communication systems with interference," *IEEE Commun. Lett.*, vol. 26, no. 9, pp. 2027–2031, Sep. 2022.
[52] M. Charishma, A. Subhash, S. Shekhar, and S. Kalyani, "Outage probability expressions for an IRS-assisted system with and without source-destination link for the case of quantized phase shifts in $\kappa - \mu$ fading," *IEEE Trans. Commun.*, vol. 70, no. 1, pp. 101–117, Jan. 2022.
[53] G. Karagiannidis, D. Zogas, N. Sagias, S. Kotsopoulos, and G. Tombras, "Equal-gain and maximal-ratio combining over nonidentical Weibull fading channels," *IEEE Trans. Wireless Commun.*, vol. 4, no. 3, pp. 841–846, May 2005.
[54] K. A. Hamdi, "Some notes on the Fourier transform methods for error-rate analysis of equal-gain combining," *IEEE Trans. Commun.*, vol. 58, no. 12, pp. 3364–3368, Dec. 2010.
[55] D. Love and R. Heath, "Equal gain transmission in multiple-input multiple-output wireless systems," *IEEE Trans. Commun.*, vol. 51, no. 7, pp. 1102–1110, Jul. 2003.
[56] J. M. Steele, *The Cauchy-Schwarz Master Class: An Introduction to the Art of Mathematical Inequalities*. Cambridge, U.K.: Cambridge Univ. Press, 2004.
[57] H. Du, J. Zhang, K. Guan, D. Niyato, H. Jiao, Z. Wang, and T. Kürner, "Performance and optimization of reconfigurable intelligent surface aided THz communications," *IEEE Trans. Commun.*, vol. 70, no. 5, pp. 3575–3593, May 2022.
[58] J. Salo, H. El-Sallabi, and P. Vainikainen, "The distribution of the product of independent Rayleigh random variables," *IEEE Trans. Antennas Propagat.*, vol. 54, no. 2, pp. 639–643, Feb. 2006.
[59] B. Lu, R. Wang, and Y. Liu, "Outage probability of intelligent reflecting surface assisted full duplex two-way communications," *IEEE Commun. Lett.*, vol. 26, no. 2, pp. 286–290, Feb. 2022.
[60] T. Chaayra, H. Ben-azza, and F. El Bouanani, "New accurate approximation for the sum of generalized Gamma distributions and its applications," *J. Appl. Math. Inform. Sciences*, vol. 14, no. 6, pp. 1121–1136, Nov. 2020.

Ahmad Massud Tota Khel received the B.Sc. degree in electrical and electronics engineering from Istanbul University, Istanbul, Turkey, and the M.Sc. degree (with Distinction) in telecommunications systems from Aston University, Birmingham, U.K. He is currently pursuing the Ph.D. degree in electrical and electronic engineering with The University of Manchester, Manchester, U.K. His research interests include design and analysis of wireless communication networks, reconfigurable intelligent surfaces, physical layer security, millimeter wave and terahertz communications, NOMA, and IoT systems.

Khairi Ashour Hamdi (Senior Member, IEEE) received the B.Sc. degree in electrical engineering from Alfateh University, Tripoli, Libya, in 1981, the M.Sc. degree (Hons.) from the Technical University of Budapest, Budapest, Hungary, in 1988, and the Ph.D. degree in telecommunication engineering from the Hungarian Academy of Sciences, Budapest, in 1993. Previously, he held research and academic posts with the Department of Computer Science, The University of Manchester, and the Department of Electronic Systems Engineering, University of Essex. He was a BT Research Fellow, in Summer 2002, and was a Visiting Assistant Professor with Stanford University, during the academic year 2007–2008. He is currently a Senior Lecturer with The University of Manchester. His current research interests include modeling and performance analysis of wireless communication systems, and networks.